Applied Thermal Engineering 119 (2017) 403–424

Contents lists available at ScienceDirect

Applied Thermal Engineering

journal homepage: www.elsevier.com/locate/apthermeng

Research Paper

Analytical investigation of heat transfer and classical entropy generation in microreactors – The influences of exothermicity and asymmetry

Graeme Hunt [a], Nader Karimi [a,*], Mohsen Torabi [b]

[a] School of Engineering, University of Glasgow, Glasgow G12 8QQ, United Kingdom
[b] The George W. Woodruff School of Mechanical Engineering, Georgia Institute of Technology, Atlanta, GA 30332, USA

HIGHLIGHTS

- Microreactors may significantly deviate from local thermal equilibrium.
- Geometrical configuration of the microstructure can majorly affect the *Nu*.
- Asymmetric thermal boundary conditions and exothermicity strongly affect the *Nu*.
- There exist certain wall thicknesses maximising heat transfer and entropy generation.
- Thermal asymmetry is a strong source of irreversibility in microreactors.

ARTICLE INFO

Article history:
Received 20 October 2016
Revised 4 February 2017
Accepted 12 March 2017
Available online 14 March 2017

Keywords:
Microreactors
Porous media
Internal heat sources
Entropy generation
Local thermal non-equilibrium

ABSTRACT

Heat transfer and entropy generation are analysed theoretically in a thermal model of microreactors accommodating processes with large heat of reaction. This includes an asymmetric, thick wall, partially-filled porous microchannel under local thermal non-equilibrium. The system features exothermicity/endothermicity within the solid and fluid phases to represent heat of chemical reactions and absorption of microwaves by the microstructure. For constant but uneven temperature boundary condition, analytical solutions are developed for the temperature profiles, Nusselt number (*Nu*) and local and total entropy generation. The influences of the system configuration and thermal specifications upon the heat transfer and irreversibilities are, subsequently, examined. This reveals the strong effects of the wall thicknesses and thermal asymmetry on the heat transfer and entropy generation of the microreactor. Most importantly, it is shown that for given exothermicities in the system there exist optimal wall and porous insert thicknesses that result in the maximum *Nu* and minimum total entropy generation. The presented analyses are therefore of practical significance and demonstrate the possibility of developing thermal and entropic optimal designs of the microstructure of microreactors.

1. Introduction

Over the last two decays there has been an increasing interest in miniaturisation in process and energy industries [1,2]. This has resulted in the development of the so-called 'microreactors' for the purpose of process intensification [1,2]. These devices build upon the technological progress in the general fields of microchannels and micro-fluids to accommodate homogenous or heterogonous chemical reactions [3,4]. Microreactors offer massively increased surface to volume ratio and highly improved transport of heat and mass, which make them attractive for the processes with large heat of reaction [5]. The volume of fluid inside the microreactor is usually very small. However, the fluid velocity in the channel may vary from few centimetres to tens of centimetres per second [6]. This together with the variations in the fluid type renders a wide range of operational parameters (e.g. Reynolds and Peclet numbers) in microreactors [6].

The applications of microreactors are now most extensive and include those in combustion [7,8], hydrogen and syngas production [9,10] and industrial chemicals [11,12]. Most of these processes involve multiple reactants and exothermic/endothermic stages. Therefore, microreactors should feature very efficient mixing and heat transfer characteristics. The fluid dynamics and mass transfer behaviours of microreactors have been already subject to significant investigations, see for example [6,13] for reviews of literature. Although there has been some works on the exchanges of heat between the microreactors and surrounding [4], the internal

* Corresponding author.
E-mail address: nader.karimi@glasgow.ac.uk (N. Karimi).

http://dx.doi.org/10.1016/j.applthermaleng.2017.03.057
1359-4311/

Nomenclature

a_{sf}	interfacial area per unit volume of porous media, m^{-1}
Bi	Biot number
Br	Brinkman number
Da	Darcy number
h_4	height of the microchannel, m
h_{sf}	fluid-to-solid heat transfer coefficient, $W\,m^{-2}\,K^{-1}$
k_1	reference thermal conductivity for lower solid material, $W \cdot m^{-1} \cdot K^{-1}$
k_2	reference thermal conductivity for upper solid material, $W \cdot m^{-1} \cdot K^{-1}$
k_{ef}	effective thermal conductivity of the fluid phase of the porous medium, $W \cdot m^{-1} \cdot K^{-1}$
k_{es}	effective thermal conductivity of the solid phase of the porous medium, $W \cdot m^{-1} \cdot K^{-1}$
k_{e1}	ratio of the porous medium thermal conductivity to the lower solid material thermal conductivity
k_{e2}	ratio of the porous medium thermal conductivity to the upper solid material thermal conductivity
Nu	Nusselt number
Q_1	dimensionless volumetric internal heat generation rate for the lower solid material
Q_2	dimensionless volumetric internal heat generation rate for the upper solid material
$\dot{q}_1$	volumetric internal heat generation rate for the lower solid material, $W \cdot m^{-3}$
$\dot{q}_2$	volumetric internal heat generation rate for the upper solid material, $W \cdot m^{-3}$
s_s	volumetric internal heat generation rate for the solid phase of the porous medium
s_f	volumetric internal heat generation rate for the fluid phase of the porous medium
T	temperature, K
T_c	outer temperature of the upper solid material, K
T_{f1}	temperature of the fluid phase of the porous medium, K
T_{f2}	temperature of the clear fluid phase, K
T_H	inner temperature of the lower solid material, K
T_s	temperature of the solid phase of the porous medium, K
T_1	temperature of the lower solid material, K
T_2	temperature of the upper solid material, K
U	dimensionless velocity of the fluid in the porous medium
U_{f1}	dimensionless velocity of the fluid in the porous medium
U_{f2}	dimensionless velocity of the fluid in the porous medium
u_{f1}	velocity of the fluid in the porous medium, $m \cdot s^{-1}$
u_{f2}	velocity of the fluid in the clear fluid, $m \cdot s^{-1}$

Greek symbols

ω_f	dimensionless volumetric internal heat generation rate for the fluid phase of the porous medium
ω_s	dimensionless volumetric internal heat generation rate for the solid phase of the porous medium
ε	porosity of the porous medium
κ	permeability, m^2
μ_{eff}	dynamic viscosity of the porous medium, $kg \cdot s^{-1} \cdot m^{-1}$
μ_f	dynamic viscosity of the base fluid, $kg \cdot s^{-1} \cdot m^{-1}$
θ	dimensionless temperature
θ_1	dimensionless temperature of the lower solid material
θ_2	dimensionless temperature of the upper solid material
θ_{f1}	dimensionless temperature of the fluid phase of the porous medium
θ_{f2}	dimensionless temperature of the clear fluid phase
θ_H	dimensionless temperature at the outer side of the lower wall
θ_s	dimensionless temperature of the solid phase of the porous medium

heat transfer aspects of these devices remain largely unexplored. This is surprising as the few existing heat transfer analyses in microreactors have already revealed that the internal heat transfer processes could significantly affect the chemical performance of the reactor [4,10]. Further, recent studies strongly emphasised the importance of microstructure design in the optimal functioning of microreactors [12]. Indeed, any detailed design of microstructure calls for comprehensive thermal analyses of microreactors under varying configuration.

Microreactors often include a collection of microchannels, in which the chemical reactions take place [2,3]. An inherent characteristic of a microchannel is the non-negligible influence of the channel walls on the thermal behaviour of the system [14,15]. Hence, a complete heat transfer analysis of any microchannel system should include heat conduction within the microchannel walls. Besides, microchannels may use porous materials for further enhancement of heat transfer [2,3]. In microreactors, porous inserts are also used to introduce catalysts and increase the rate of mass transfer [12,16]. Typically, these porous inserts are attached to the walls of the channel and may vary in thickness and structural characteristics. Such configuration has been investigated by Chein and co-workers in a series of numerical studies [17–19]. In these works the equations governing the transport of momentum, heat and chemical species along with the key reactions for the reforming of methanol were solved simultaneously. The transport of heat in the porous region of the reactor was modelled on the basis of the local thermal equilibrium (LTE) model and the thermal effect of exothermic/endothermic catalytic reactions was represented by a volumetric energy source term [17]. The resultant temperature of the fluid phase and the rate of syngas production were then reported. The main purpose of these works was to understand the combined effects of heat, mass and momentum transfer in the microreactor upon the reforming process. Although the significance of the temperature fields was well demonstrated [18,20], no detailed heat transfer analysis and Nusselt number (Nu) evaluation was conducted in these investigations. The latter is of primary importance in microreactors as their proper operation is often subject to an efficient exchange of heat with an external heat sink or source [4,21]. Further, the recent advancements in the field of heat convection in partially-filled porous conduits have revealed the strong effects of exothermicity on the temperature profiles and heat transfer rates within the system. In their recent theoretical studies, Karimi et al. [22] and Torabi et al. [23,24] considered internal heat sources in partially-filled porous channels with varying configurations. They solved the problem under local thermal non-equilibrium (LTNE) and compared the results with those of the corresponding local thermal equilibrium analyses (LTE). This showed that the introduction of heat sources in porous conduits could significantly undermine the assumption of local thermal equilibrium. Hence, the temperature profiles and Nu calculations under LTE can be highly erroneous and conduction of LTNE analysis is an essential necessity in any

accurate heat transfer study of these systems. Most recently, these conclusions were further extended to nanofluid-porous systems with internal heat generations [25,26].

In another recent development, it was shown that the inclusion of thick walls of the conduit in the heat transfer analysis of microchannels results in very pronounced modifications of their thermal behaviour. Ibáñez et al. [27] considered the problem of heat and fluid flow in a microchannel with thick walls. Here, constant thermal conductivity for the solid walls was assumed, and analytical expressions for the velocity and temperature fields were derived [27]. Theoretical works of Torabi et al. [15,28] on forced convection in porous microchannels showed that the finite thickness of the channel walls could significantly influence the thermal and entropic behaviours of the system. Most recently, Elliott et al. [29] investigated the thermal behaviour of a porous channel with thick walls subject to asymmetric thermal boundary conditions and internal heat sources. This work considered LTNE condition and showed that the temperature fields and *Nu* of the system are strongly affected by the thickness of the wall and asymmetry of the boundary conditions [29]. It follows from the works of Torabi et al. [15,28] and Elliot et al. [29] that ignoring the wall thickness in porous channels and microchannels could lead to the introduction of significant errors in the calculated temperature fields and *Nu*. As stated earlier, such errors may introduce major problems in the design and operation of microreactors. Currently, the extent of wall influences upon the thermal behaviour of the partially-filled porous microchannels is still unclear. In particular, there is little comprehension on the effects of exothermicity, local non-equilibrium and thick asymmetric channel walls, while coexistence of these effects is common in microreactors.

Entropy generation minimisation is now employed widely in the design and optimisation of various thermal and thermochemical systems [30,31]. These include porous systems under LTE [32,33] and LTNE [34,35] and have been also recently extended to solid systems [31]. Investigation of the local and total entropy production highlights the sources and locations of irreversibilities, and hence illustrates the necessary design modifications [31]. The second law analyses of forced convection of heat in porous media have shown that compared to hydrodynamic irreversibilities, thermal effects have a relatively larger share of the total irreversibility of the system [31,32,34]. This finding is more pronounced for the systems under LTNE [23–26]. Expectedly, thermal irreversibilities are very strong in exothermic porous systems and are dominated by the intensity of exothermicity [23,24]. Entropy generation in micro-combustors have been conducted in the past, e.g. [36–38]. Nonetheless, to the best of authors' knowledge this was never extended to other microreactors and in particular to those with porous inserts. Ideally, entropic analysis of a microreactor should include the irreversibilities by the thermal and viscous effects, mass transfer and chemical reactions. Yet, investigations of entropy generation in highly exothermic reactive flows have indicated that the total irreversibility is dominated by the thermal effects [39]. It is, therefore, expected that in microreactors exothermicity of the reactions and heat transfer characteristics of the system govern the rate of the entropy generation.

The preceding discussions can be summarised by the followings.

- Microreactors may feature an extensive range of operating parameters. In particular, their Peclet and Reynolds number extend over several orders of magnitude and include extremely low values (of order of 0.01 and less [6]).
- Heat transfer plays an essential role in the operation of many microreactors [4]. However, comprehensive heat transfer analyses of microreactors with the inclusion of thick walls and non-equilibrium effects are infrequent and most of the existing thermal studies are limited to temperature estimations [17–20].
- Microreactors normally use porous media to introduce catalysts and enhance the transfer of heat and mass. Conventionally, thermal analysis of porous media in microreactors includes LTE assumptions [17]. However, recent investigations have shown that this assumption could be largely wrong in the presence of strong exothermicity [22–24]. Currently, LTNE analyses of thick wall microchannels partially-filled with porous media and featuring exothermicity (similar to what happens in microreactors) do not exist.
- All the existing thermal analyses of microreactors took a first law approach and entropy generation studies in microreactors are yet to be conducted.
- It has been already demonstrated that in exothermic reactive systems the thermal irreversibility is the most significant source of the entropy generation [23,24,39].

Given these points, the current study aims to provide an analytical view of the first and second law behaviours of a simple, yet representative, model of a microreactor with highly exothermic or endothermic reactions. The focus of the study is on the thermal aspects and hence mass transfer and reactions are ignored, while the effects of the latter are represented by an energy source term. Further, the influences of the absorption of microwaves or infrared waves [40] are represented by another energy source term within the solid phase of the microstructure. The composite system, including a partial porous insert and thick asymmetric walls, is then analysed theoretically through a local non-equilibrium approach.

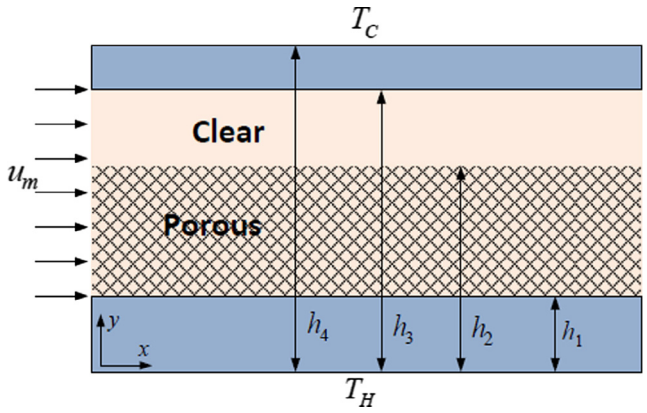

Fig. 1. Schematic view of the model microreactor with thick walls and porous insert.

2. Analytical method

2.1. Problem configuration and assumptions

Fig. 1 shows a schematic view of the problem under investigation. The fluid (reactants) enters a two-dimensional microchannel confined between parallel slabs of solid with different thicknesses and subject to constant but unequal temperatures on the external surfaces. The channel is partially-filled by a porous insert attached to the lower wall. The thickness of this insert varies and so does the thickness of the thick walls. The configuration under investigation is therefore geometrically and thermally asymmetric. The existence of porous insert significantly increases the thermal diffusivity of the microchannel. Also, low fluid velocity is common in many exothermic processes in microreactors [6]. As a result, the thermal Peclet number of the system shown in Fig. 1 is expected to be quite

low ($Pe_{th} \ll 1$). Under this condition, the axial advection of heat becomes negligible in comparison with the transversal heat transfer by internal heat convection in the porous medium and conduction in the fluid and solid components of the system. This assumption was first introduced and rigorously justified by Mahmud and Fraser [41] and more recently was employed by a large number of authors [28,29,42–44].

The following assumptions are, further, made throughout the current study.

- The thermal model of microreactor, shown in Fig.1, excludes mass transfer and chemical reactions and is exclusively concerned with the hydrodynamic, thermal and entropic behaviours of the system.
- The porous medium is homogenous, isotropic and fluid saturated. The fluid phase features uniform and steady internal heat generation/consumption, which represents exothermicity/endothermicity of the chemical reactions [17]. The solid phase also includes internal heat generation representing absorption of microwave and infrared waves [40,45].
- The fluid flow is steady, laminar, viscous and incompressible, satisfying the no-slip boundary conditions on the wall. Further, thermally and hydrodynamically fully developed conditions hold in both open and porous regions. Furthermore, physical properties such as porosity, specific heat, density and thermal conductivities are invariants and thermal dispersion effects are ignored [46,47].
- Due to the submillimeter transverse dimension of the system, the Rayleigh number and therefore natural convection effects are negligibly small. Further, thermal emissivity is assumed small and radiative heat transfer is ignored.
- The current analysis is concerned with those processes, which feature volumetrically almost uniform reactions [17–19]. Processes with abrupt reaction zones, separating hot and cold flows, such as those encountered in micro-combustion [48] are not considered. As a result, the axial conduction of heat within the walls is not essential and is ignored throughout the analysis. This is further justified by noting that experimental investigations [7,13,49] revealed that the axial temperature gradient within the microstructure diminishes in thick wall microreactors. Hence, the axial heat conduction in the configuration shown in Fig.1 is insignificant.

2.2. Governing equations and analytical solutions

Employing Darcy-Brinkman model, the equations for the transport of momentum in the porous and clear regions, respectively, are given by

$$-\frac{\partial p}{\partial x}+\mu_{eff}\frac{\partial^2 u_{f1}}{\partial y^2}-\frac{\mu_f}{\kappa}u_{f1}=0 \quad h_1 \leqslant y < h_2 \tag{1a}$$

$$-\frac{\partial p}{\partial x}+\mu_f\frac{\partial^2 u_{f2}}{\partial y^2}=0 \quad h_2 \leqslant y < h_3 \tag{1b}$$

Transport of thermal energy for the components of the system including to the lower wall, the fluid and solid phases in the porous region, the clear fluid above the porous region and the upper wall, respectively, are expressed by the following equations.

$$k_1\frac{d}{dy}\left[\frac{dT_1}{dy}\right]+\dot{q}_1=0 \quad 0 < y \leqslant h_1 \tag{2a}$$

$$k_{ef}\frac{\partial^2 T_{f1}}{\partial y^2}+h_{sf}a_{sf}(T_s-T_{f1})+s_f=\rho C_p u_{f1}\frac{\partial T_{f1}}{\partial x} \quad h_1 \leqslant y < h_2 \tag{2b}$$

$$k_{es}\frac{\partial^2 T_s}{\partial y^2}+h_{sf}a_{sf}(T_s-T_{f1})+s_s=0 \quad h_1 \leqslant y < h_2 \tag{2c}$$

$$k_f\frac{\partial^2 T_{f2}}{\partial y^2}+s_f=\rho C_p u_{f2}\frac{\partial T_{f2}}{\partial x} \quad h_2 \leqslant y < h_3 \tag{2d}$$

$$k_2\frac{d}{dy}\left[\frac{dT_2}{dy}\right]+\dot{q}_2=0 \quad h_3 \leqslant y < h_4 \tag{2e}$$

As discussed in Section 2.1, the advection terms on the right hand side of Eqs. (2b) and (2d) become vanishingly small when compared to the conduction and internal convection terms. Hence the advection terms are ignored in the current analysis. This results in the transformation of the governing equations to the followings.

$$k_1\frac{d}{dy}\left[\frac{dT_1}{dy}\right]+\dot{q}_1=0 \quad 0 < y \leqslant h_1 \tag{3a}$$

$$k_{ef}\frac{d^2 T_{f1}}{dy^2}+h_{sf}a_{sf}(T_s-T_{f1})+s_f=0 \quad h_1 \leqslant y < h_2 \tag{3b}$$

$$k_{es}\frac{d^2 T_s}{dy^2}+h_{sf}a_{sf}(T_s-T_{f1})+s_s=0 \quad h_1 \leqslant y < h_2 \tag{3c}$$

$$k_f\frac{d^2 T_{f2}}{dy^2}+s_f=0 \quad h_2 \leqslant y < h_3 \tag{3d}$$

$$k_2\frac{d}{dy}\left[\frac{dT_2}{dy}\right]+\dot{q}_2=0 \quad h_3 \leqslant y < h_4 \tag{3e}$$

The upper and lower boundary conditions can be written as:

$$y=h_4 \quad T_2=T_C \tag{4a}$$

$$y=0 \quad T_1=T_H \tag{4b}$$

The following three conditions representing the interfaces are required for closure of the system [23,24,29].

$$y=h_1: \quad u_{f1}=0, \quad T_1=T_s=T_{f1}, \quad k_1\left.\frac{dT_1}{dy}\right|_{y=h_1}=k_{ef}\left.\frac{dT_{f1}}{dy}\right|_{y=h_1}+k_{es}\left.\frac{dT_s}{dy}\right|_{y=h_1} \tag{5a}$$

$$y=h_2: \quad \mu_{eff}\frac{\partial u_{f1}}{\partial y}=\mu_f\frac{\partial u_{f2}}{\partial y}, \tag{5b}$$

$$y=h_2: \quad u_{f1}=u_{f2}, \quad T_{f2}=T_s=T_{f1}, \quad k_f\left.\frac{dT_{f2}}{dy}\right|_{y=h_2}=k_{ef}\left.\frac{dT_{f1}}{dy}\right|_{y=h_2}+k_{es}\left.\frac{dT_s}{dy}\right|_{y=h_2} \tag{5c}$$

$$y=h_3: \quad u_{f2}=0, \quad T_2=T_{f2}, \quad k_2\left.\frac{dT_2}{dy}\right|_{y=h_3}=k_{ef}\left.\frac{dT_{f1}}{dy}\right|_{y=h_3} \tag{5d}$$

In this system, the Nu can be written in the following form [23,24]:

$$Nu=\frac{2(h_3-h_1)q_w}{k_f(T_{f1,w}-T_{f,m})} \tag{6}$$

where

$$T_{f,m}=\frac{1}{(h_3-h_1)u_m}\left(\int_{h_1}^{h_2}u_{f1}T_{f1}dy+\int_{h_2}^{h_3}u_{f2}T_{f2}dy\right) \tag{7a}$$

$$u_m = \frac{1}{(h_3 - h_1)}\left(\int_{h_1}^{h_2} u_{f1}dy + \int_{h_2}^{h_3} u_{f2}dy\right) \tag{7b}$$

$$q_w = k_1 \left.\frac{dT_1}{dy}\right|_{y=h_1} \tag{7c}$$

The resultant equations for the local entropy rate across all components of the system can be written as follows [23,24,31].

$$\dot{S}''' = \begin{cases} \frac{k_1}{T_1^2}\left(\frac{dT_1}{dy}\right)^2 & 0 < y < h_1 \\ \frac{k_{sf}}{T_{f1}^2}\left(\frac{dT_{f1}}{dy}\right)^2 + \frac{h_{sf}a_{sf}(T_s - T_{f1})^2}{T_s T_{f1}} + \frac{\mu_f}{\kappa T_{f1}}u_{f1}^2 + \frac{\mu_{eff}}{T_{f1}}\left(\frac{\partial u_{f1}}{\partial y}\right)^2 & h_1 < y < h_2 \\ \frac{k_{es}}{T_s^2}\left(\frac{dT_s}{dy}\right)^2 + \frac{h_{sf}a_{sf}(T_s - T_{f1})^2}{T_s T_{f1}} & h_1 < y < h_2 \\ \frac{k_f}{T_{f2}^2}\left(\frac{dT_{f2}}{dy}\right)^2 + \frac{\mu_f}{T_{f2}}\left(\frac{\partial u_{f2}}{\partial y}\right)^2 & h_2 < y < h_3 \\ \frac{k_2}{T_2^2}\left(\frac{dT_2}{dy}\right)^2 & h_3 < y < h_4 \end{cases} \tag{8}$$

It is noted that the thermal energy source terms do not explicitly appear in Eq. (8). Yet, they indirectly affect the entropy generation through altering the temperature fields. An extensive discussion on this subject can be found in a recent review by Torabi et al. [31].

The following dimensionless parameters are introduced to enable further physical analysis.

$$\begin{aligned} &\theta_1 = \tfrac{T_1}{T_C},\ \theta_s = \tfrac{T_s}{T_C},\ \theta_{f1} = \tfrac{T_{f1}}{T_C},\ \theta_{f2} = \tfrac{T_{f2}}{T_C},\ \theta_2 = \tfrac{T_2}{T_C},\ \theta_H = \tfrac{T_H}{T_C},\ Y = \tfrac{y}{h_4}, \\ &Y_1 = \tfrac{h_1}{h_4},\ Y_2 = \tfrac{h_2}{h_4},\ Y_3 = \tfrac{h_3}{h_4},\ Q_1 = \tfrac{\dot{q}_1 h_4^2}{k_1 T_C},\ Q_2 = \tfrac{\dot{q}_2 h_4^2}{k_2 T_C},\ \omega_s = \tfrac{s_s h_4^2}{k_{es} T_C}, \\ &\omega_f = \tfrac{s_f h_4^2}{k_{es} T_C},\ U_{f1} = \tfrac{u_{f1}}{u_r},\ U_{f2} = \tfrac{u_{f2}}{u_r},\ u_r = -\tfrac{h_4^2}{\mu_f}\tfrac{\partial p}{\partial x},\ k = \tfrac{k_{es}}{k_{ef}} = \tfrac{(1-\varepsilon)k_s}{\varepsilon k_f}, \\ &Bi = \tfrac{h_{sf}a_{sf}h_4^2}{k_{es}},\ Br = \tfrac{\mu_f u_r^2}{T_C k_{es}},\ k_{e1} = \tfrac{k_{ef}}{k_1},\ k_{e2} = \tfrac{k_{ef}}{k_2},\ Da = \tfrac{\kappa}{h_4^2}. \end{aligned} \tag{9}$$

Substituting the above parameters into the governing Eqs. (1a) and (1b) and Eqs. (3a)(3e), results in the non-dimensional equations for the transport of momentum and thermal energy.Applying parameters from Eq. (9) to the momentum Eqs. (1a) and (1b) results in the following dimensionless forms.

$$1 + \frac{1}{\varepsilon}\frac{d^2U_{f1}}{dY^2} - \frac{U_{f1}}{Da} = 0 \quad Y_1 < Y \leqslant Y_2 \tag{10a}$$

$$1 + \frac{d^2U_{f2}}{dY^2} = 0 \quad Y_2 < Y \leqslant Y_3 \tag{10b}$$

The equations for the transport of heat (Eqs. (3ae)) reduce to the followings

$$\frac{d}{dY}\left[\frac{d\theta_1}{dY}\right] + Q_1 = 0 \quad 0 < Y \leqslant Y_1 \tag{11a}$$

$$\frac{1}{k}\frac{d^2\theta_{f1}}{dY^2} + Bi(\theta_s - \theta_{f1}) + \omega_f = 0 \quad Y_1 < Y \leqslant Y_2 \tag{11b}$$

$$\frac{d^2\theta_s}{dY^2} - Bi(\theta_s - \theta_{f1}) + \omega_s = 0 \quad Y_1 < Y \leqslant Y_2 \tag{11c}$$

$$\frac{1}{\varepsilon k}\frac{d^2\theta_{f2}}{dY^2} + \omega_f = 0 \quad Y_2 < Y \leqslant Y_3 \tag{11d}$$

$$\frac{d}{dY}\left[\frac{d\theta_2}{dY}\right] + Q_2 = 0 \quad Y_3 < Y \leqslant 1 \tag{11e}$$

Furthermore, the thermal boundary conditions on the outer edges of the walls, Eqs. (4a) and (4b) become:

$$Y = 0: \quad \theta_1 = \theta_H \tag{12a}$$

$$Y = 1: \quad \theta_2 = 1 \tag{12b}$$

Whereas the thermal and hydrodynamic interface conditions (5a)(5d) reduce to:

$$Y = Y_1: \quad U = 0 \quad \theta_1 = \theta_s = \theta_{f1} \quad \left.\frac{d\theta_1}{dY}\right|_{Y=Y_1} = k_{e1}\left.\frac{d\theta_{f1}}{dY}\right|_{Y=Y_1} + kk_{e1}\left.\frac{d\theta_s}{dY}\right|_{Y=Y_1} \tag{13a}$$

$$Y = Y_2: \quad U_{f1} = U_{f2} \quad \theta_{f1} = \theta_s = \theta_{f2} \quad \left.\frac{d\theta_{f2}}{dY}\right|_{Y=Y_2} = \varepsilon\left.\frac{d\theta_{f1}}{dY}\right|_{Y=Y_2} + k\varepsilon\left.\frac{d\theta_s}{dY}\right|_{Y=Y_2} \tag{13b}$$

$$Y = Y_3: \quad U = 0 \quad \theta_2 = \theta_{f2} \quad \left.\frac{d\theta_2}{dY}\right|_{Y=Y_3} = \frac{k_{e2}}{\varepsilon}\left.\frac{d\theta_{f2}}{dY}\right|_{Y=Y_3} \tag{13c}$$

$$Y = Y_2: \quad \frac{1}{\varepsilon}\frac{\partial U_{f1}}{\partial Y} = \frac{\partial U_{f2}}{\partial Y} \tag{13d}$$

Utilising the dimensionless parameters in Eq. (9), the dimensionless *Nu* is given by the following relations.

$$Nu = \frac{2\varepsilon(Y_3 - Y_1)}{k_{e1}(\theta_{f1}(Y_1) - \theta_{f,m})}\left.\frac{d\theta_1}{dY}\right|_{Y=Y_1} \tag{14}$$

where

$$\theta_{f,m} = \frac{1}{(Y_3 - Y_1)U_m}\left(\int_{Y_1}^{Y_2} U_{f1}\theta_{f1}dY + \int_{Y_2}^{Y_3} Y_{f2}\theta_{f2}dY\right) \tag{15a}$$

$$U_m = \frac{1}{(Y_3 - Y_1)}\left(\int_{Y_1}^{Y_2} U_{f1}dY + \int_{Y_2}^{Y_3} U_{f2}dY\right) \tag{15b}$$

$$Q_w = \left.\frac{d\theta_1}{dY}\right|_{Y=Y_1} \tag{15c}$$

Upon normalisation using the dimensionless variables given in Eq. (9) the dimensionless local volumetric entropy generation rate, N_S is given by:

$$N_s = \begin{cases} \frac{1}{\theta_1^2}\left(\frac{d\theta_1}{dY}\right)^2 & 0 < Y < Y_1 \\ \frac{k_{e1}}{\theta_{f1}^2}\left(\frac{d\theta_{f1}}{dY}\right)^2 + \frac{kk_{e1}Br(\theta_s - \theta_{f1})^2}{\theta_s\theta_{f1}} + \frac{kk_{e1}BrU_{f1}^2}{Da\theta_{f1}} + \frac{kk_{e1}Br}{T_{f1}}\left(\frac{dU_{f1}}{dY}\right)^2 & Y_1 < Y < Y_2 \\ \frac{kk_{e1}}{\theta_s^2}\left(\frac{d\theta_s}{dY}\right)^2 + \frac{kk_{e1}Bi(\theta_s - \theta_{f1})^2}{\theta_s\theta_{f1}} & Y_1 < Y < Y_2 \\ \frac{k_{e1}}{\varepsilon\theta_{f2}^2}\left(\frac{d\theta_{f2}}{dY}\right)^2 + \frac{kk_{e1}Br}{\theta_{f2}}\left(\frac{dU_{f2}}{dY}\right)^2 & Y_2 < Y < Y_3 \\ \frac{k_{e1}}{k_{e2}\theta_2^2}\left(\frac{d\theta_2}{dY}\right)^2 & Y_3 < Y < Y_4 \end{cases} \tag{16}$$

Finally, the dimensionless volumetric averaged entropy generation rate, N_t is defined as

$$N_t = \int_0^1 N_s\, dY. \tag{17}$$

2.2.1. Velocity profiles

The normalised velocity equation for the clear fluid region Eq. (10b) is readily solved to reveal the following velocity profile,

$$U_{f2} = \frac{-Y^2}{2} + A_1 Y + A_2. \tag{18a}$$

Nevertheless, Eq. (10a) is more complicated and its analytical solution results in the following velocity profile for the fluid in the porous region:

$$U_{f1} = -\frac{2((2A_2 - 2Da + 2A_1Y_2 - Y_2^2)\cosh\left(\frac{z}{2}(Y - Y_1)\right) + \cosh\left(\frac{z}{2}(Y + Y_1 - 2Y_2)\right)\sinh\left(\frac{z}{2}(Y - Y_1)\right)(\cosh(z(Y_1 + Y_2)) + \sinh(z(Y_1 + Y_2)))}{\cosh(2zY_1) - \cosh(2zY_2) + \sinh(2zY_1) - \sinh(2zY_2)}, \tag{18b}$$

where A_1 and A_2 are constants and $z = \frac{\sqrt{\varepsilon}}{\sqrt{Da}}$.

2.2.2. Temperature profiles

Eqs. (11b) and (11c) may be decoupled by increasing the order of derivatives to form a new set of differential equations in a manner that each equation contains only one dependent variable, either θ_s or θ_{f1}. This gives rise to the following decoupled equations for the solid and fluid phases, respectively.

$$\theta_s''''(Y) - \mathrm{Bi}(k+1)\theta_s''(Y) - \mathrm{Bi}k(\omega_f + \omega_s) = 0 \tag{19}$$

$$\theta_{f1}''''(Y) - \mathrm{Bi}(k+1)\theta_{f1}''(Y) - \mathrm{Bi}k(\omega_f + \omega_s) = 0 \tag{20}$$

Since these equations are fourth order in θ_s and θ_{f1}, two more boundary conditions for each of θ_s and θ_{f1} are required for the closure of the system. The first of each of these is obtained by evaluating the second order derivative terms of Eqs. (11b) and (11c) at $Y = Y_2$ and applying the conditions of Eq. (13b) to yield

$$\theta_{f1}''(Y_2) = -k\omega_f, \quad \theta_s''(Y_2) = -\omega_s. \tag{21}$$

Obtaining the remaining conditions requires taking the derivative of Eqs. (11b) and (11c) with respect to Y and evaluating them at $Y = Y_2$. After some algebraic manipulations, the following equations are obtained to complete the closure of the system:

$$\theta_{f1}'''(Y_2) = -Bik\left(\theta_s'(Y_2)(1+k) - \frac{1}{\varepsilon}\theta_{f2}'(Y_2)\right) \tag{22a}$$

$$\theta_s'''(Y_2) = Bi\left(\theta_s'(Y_2)(1+k) - \frac{1}{\varepsilon}\theta_{f2}'(Y_2)\right) \tag{22b}$$

The system of Eqs. (11a), (11d), (11e), (19) and (20) can now be solved analytically. The resulting general solutions for the temperature distributions in the lower solid wall, the porous solid phase, the fluid inside porous phase, the clear fluid and the upper solid wall are, respectively, governed by:

$$\theta_1(Y) = \frac{1}{2}(-Q_1Y^2 + 2\theta_H + 2B_1Y) \tag{23a}$$

$$\theta_s(Y) = -\frac{k(\omega_f + \omega_s)Y^2}{2(1+k)} + \frac{e^{\alpha Y}B_2}{\alpha^2} + \frac{e^{-\alpha Y}B_3}{\alpha^2} + B_4 + B_5Y \tag{23b}$$

$$\theta_{f1}(Y) = -\frac{k(\omega_f + \omega_s)Y^2}{2(1+k)} + \frac{e^{\alpha Y}B_6}{\alpha^2} + \frac{e^{-\alpha Y}B_7}{\alpha^2} + B_8 + B_9Y \tag{23c}$$

$$\theta_{f2}(Y) = -\frac{1}{2}k\omega_f\varepsilon Y^2 + B_{10} + 2B_{11}Y \tag{23d}$$

$$\theta_2(Y) = \frac{1}{2}(-Q_2Y^2 + Y(2 + Q_2 - 2B_{12}) + 2B_{12}) \tag{23e}$$

where B_1 to B_{12} are constants and $\alpha = \sqrt{Bi(k+1)}$.

In order to find the particular solutions to the above equations, the boundary and interface conditions (Eqs. (12), (13), (21) and (22)) need to be used. The algebraic manipulations required to elucidate the coefficients for Eqs. (23ae) are rather substantial. To handle this, Wolfram Mathematica was employed to solve the expressions analytically and deliver the constants listed above. These constants are particularly involved and very lengthy whilst simultaneously not particularly enlightening and therefore are not shown here.

2.2.3. LTE temperature solution

In order to obtain the LTE equations governing the temperature distribution of the system in the porous region, it is first necessary to add Eqs. (11b) and (11c). This results in

$$\frac{1}{k}\theta_{f1}'' + \theta_s'' + \omega_f + \omega_s = 0. \tag{24}$$

Local thermal equilibrium condition implies the temperature of the solid and fluid phases of the porous medium are equal. Thus, $\theta_s = \theta_{f1} = \theta_p$, where θ_p is the temperature function of the porous medium under LTE condition. This permits expressing the one-equation model as

$$\left(\frac{1}{k} + 1\right)\theta_P'' + \omega_f + \omega_s = 0. \tag{25}$$

Eq. (25) is subject to the following boundary conditions

$$\theta_1(Y_1) = \theta_P(Y_1), \tag{26a}$$

$$\theta_{f2}(Y_2) = \theta_P(Y_2), \tag{26b}$$

$$\theta_{f2}'(Y_2) = (\varepsilon + \varepsilon k)\theta_P'(Y_2), \tag{26c}$$

$$\theta_1'(Y_1) = (k_{e1} + kk_{e1})\theta_P'(Y_1). \tag{26d}$$

Rearranging and integrating Eq. (25) and applying boundary conditions (26a)(26d) yields the LTE temperature distribution, which reads

$$\theta_P(Y) = -\frac{k(\omega_f + \omega_s)Y^2}{2(1+k)} + C_{3P}Y + C_{4P}, \tag{27}$$

where C_{3P} and C_{4P} are constants, which result from the integration of Eq. (25) and uncovered by applying the boundary conditions (26a) and (26b). They are not shown here in expanded form as they are substantial and the included details do not serve to further illuminate.

2.2.4. Validation

It is well established that by increasing the internal heat exchanges within the porous insert the temperature difference between the solid and fluid phases diminishes [22,50]. Thus, under this condition, the system is brought towards local thermal equilibrium. The Biot number (Bi) is a measure of internal heat exchanges in the porous medium and therefore at high Biot numbers the LTE and LTNE solutions presented in Sections 2.2.2 and 2.2.3 should approach each other. This validation method has been

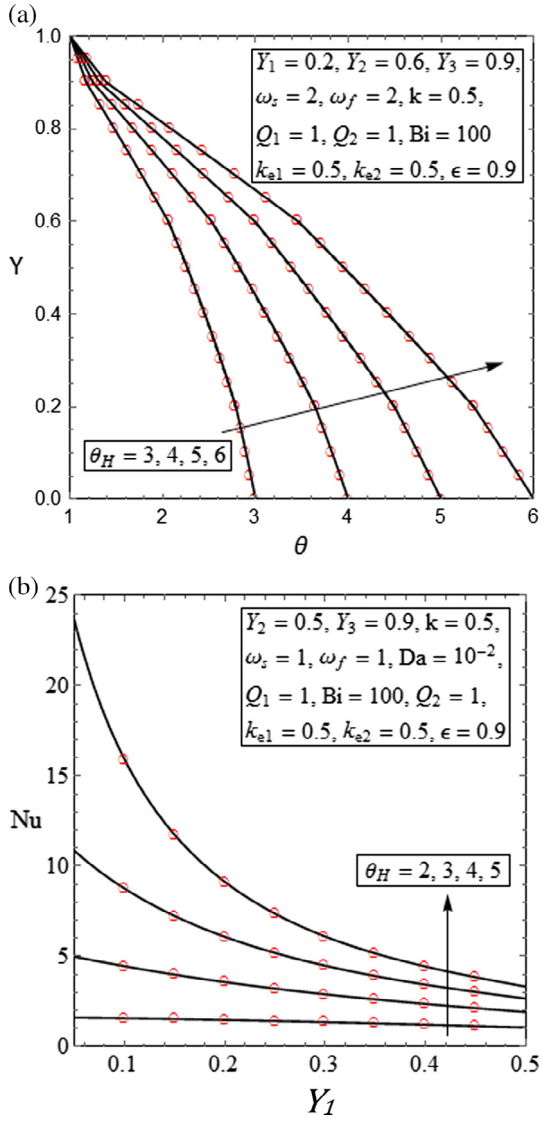

Fig. 2. (a) Temperature distribution showing LTNE solution as solid black line and LTE solution as red dots for various values of the lower wall temperature, θ_H. (b) Variation in *Nu* versus varying lower wall thickness, with the LTNE solution as the solid black line and the LTE solution as the red dots for various values of the lower wall temperature, θ_H.

Table 1
Summary of the internal heat generations in the investigated test cases.

	ω_s	ω_f
Case 1	2	0
Case 2	0	2
Case 3	2	2
Case 4	0	0

employed previously in the analyses of similar problems, e.g. [29], and can be also used in the current theoretical work. Fig. 2a shows the solid phase temperature profile across the system derived through LTNE calculations at *Bi* = 100 and compare those with their corresponding values calculated under LTE assumption. A similar comparison is made in Fig. 2b for the LTE and LTNE models to calculate *Nu*. Different values of the surface temperature ratio have been considered in these figures. The excellent agreements between the two approaches observed in Fig. 2a and b confirm the validity of the mathematical solutions of Section 2.2.

3. Results and discussions

The problem under investigation is applied to four main test cases on the basis of the exothermicity source terms. Table 1 summarises these cases. Case 1 includes a source term in the solid phase of the porous medium and no exothermicity in the fluid. This case is a representation of the processes enhanced by external radiation of microwaves or other sources of electromagnetic waves [40,45]. In case 2, heat is generated within the fluid phase, which represents a large group of exothermic or endothermic chemical reactions [2]. In case 3, both solid and fluid phases include thermal energy source terms. Case 4, however, is a model of a microchannel flow without any thermochemical activity. This provides a basic test case for comparison with the other three cases. In all of the temperature and local entropy generation plots provided in this investigation, the solid line is the specification of the system for the solid phase in that point, and the dashed line is the specification of the system for the fluid phase. Needless to say that in the porous medium of the microchannel, as LTNE model has been used, both solid and dashed lines are seen. Further, throughout the proceeding discussions the thickness of different components of the system are specified indirectly through determining the values of the three parameters h_1, h_2 and h_3 (see Fig. 1).

3.1. Temperature distributions and the validity of local thermal equilibrium

The hydrodynamics of configuration shown in Fig. 1 has been previously analysed by Torabi et al. [51]. In short, the velocity distribution includes zero velocity on the walls and smooth transition from channel flow to that in the porous insert. Further discussion about the hydrodynamics of the problem can be found in Refs. [51,52] and is not repeated here.

Geometrical configuration of the microchannel is expected to strongly affect the temperature distributions within the system. Figs. 3–5 investigate the extent of these effects through varying the thicknesses of the lower wall (Fig. 3), the porous insert (Fig. 4) and the upper wall (Fig. 5). These figures show the profile of the non-dimensional solid and fluid temperatures across the system under the four test cases specified in Table 1 and a similar set of other parameters. The temperature profiles of the entire system have been shown in parts a-d of Figs. 3–5, while parts e-h of the same figures are focused on the porous region. Figs. 3d, 4d and 5d (and also 3–5 h) clearly show that for case 4 with no exothermicity, the temperature profile features a simple behaviour under all investigated configurational variations. This includes a linear temperature distribution in all components of the system, which is a manifestation of classical conductive systems. Further, the fluid and solid temperature difference always remains negligible implying the domination of LTE in this particular case. However, the situation is significantly altered by the introduction of exothermicity in test cases 1–3. Addition of internal heat generation to the solid phase of the porous insert, in case 1, makes this phase hotter than the adjacent fluid phase. This behaviour can be equally seen in Figs. 3a–5a. Increasing the lower wall thickness in Fig. 3a and e and that of porous insert in Fig. 4a and e reduces the temperature difference between the solid and fluid phases and therefore the system approaches local equilibrium state. The same applies to Fig. 4a and e, in which as the thickness of the porous insert increases and the total volume of the microchannel is occupied by the porous material LTE becomes more dominant. However, although still existing, this trend is less pronounced in

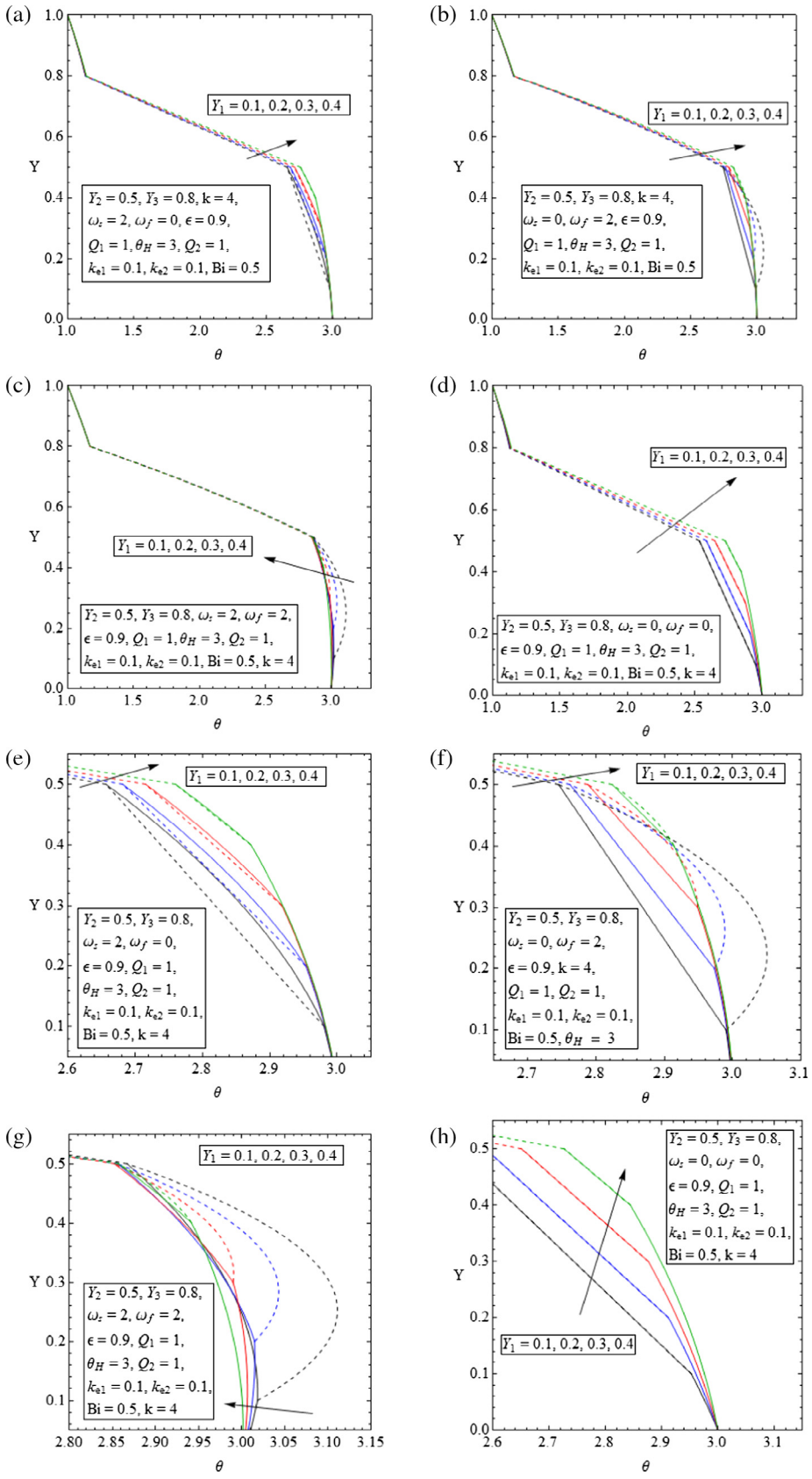

Fig. 3. Temperature distribution with various values of the lower wall thickness number, Y_1 (a–d) and focussing on the porous region (e–h), (a & e) Case 1, (b & f) Case 2, (c & g) Case 3, and (d & h) Case 4.

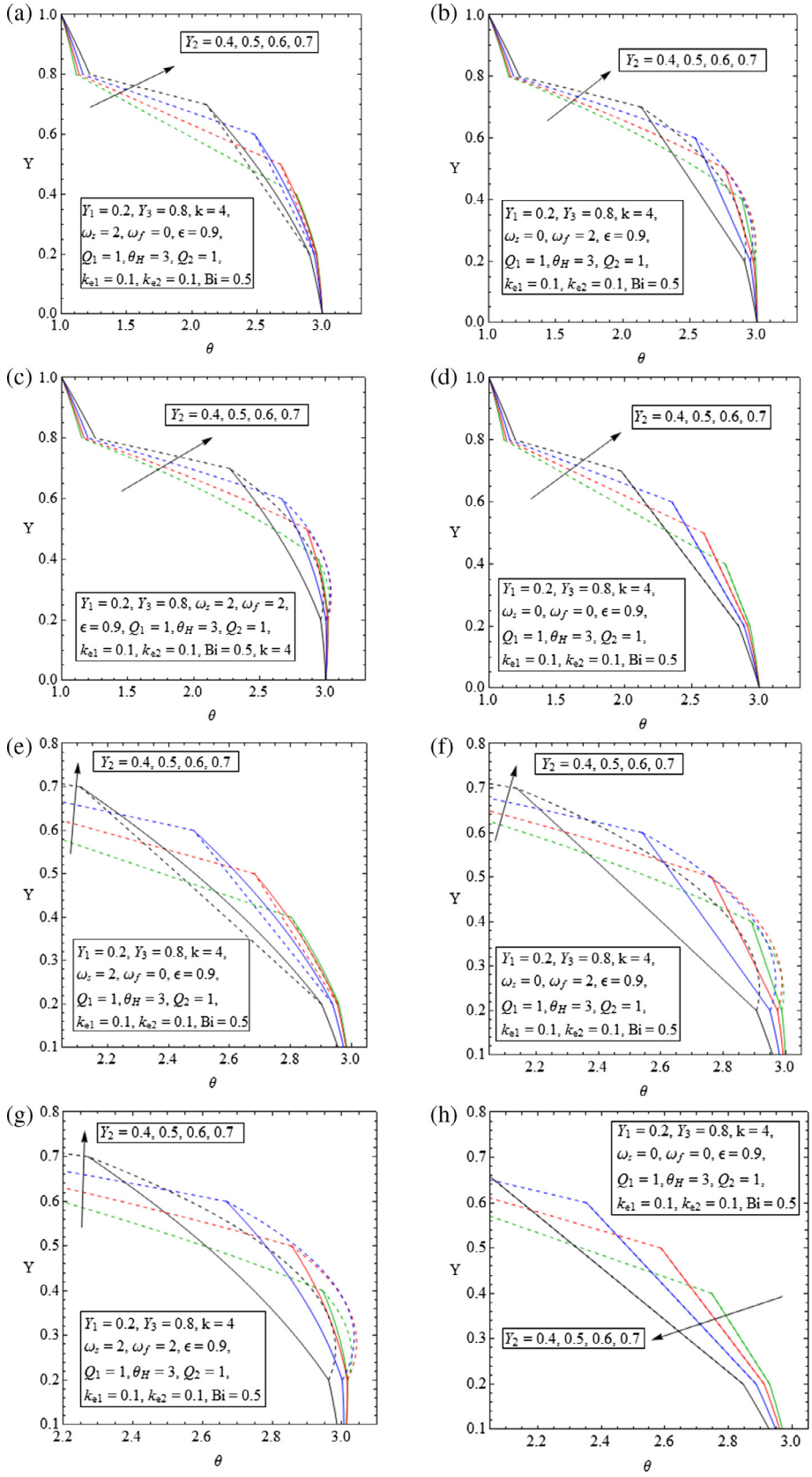

Fig. 4. Temperature distribution with various values of porous insert thickness, Y_2 (a–d) and focussing on the porous region (e–h), (a & e) Case 1, (b & f) Case 2, (c & g) Case 3, and (d & h) Case 4.

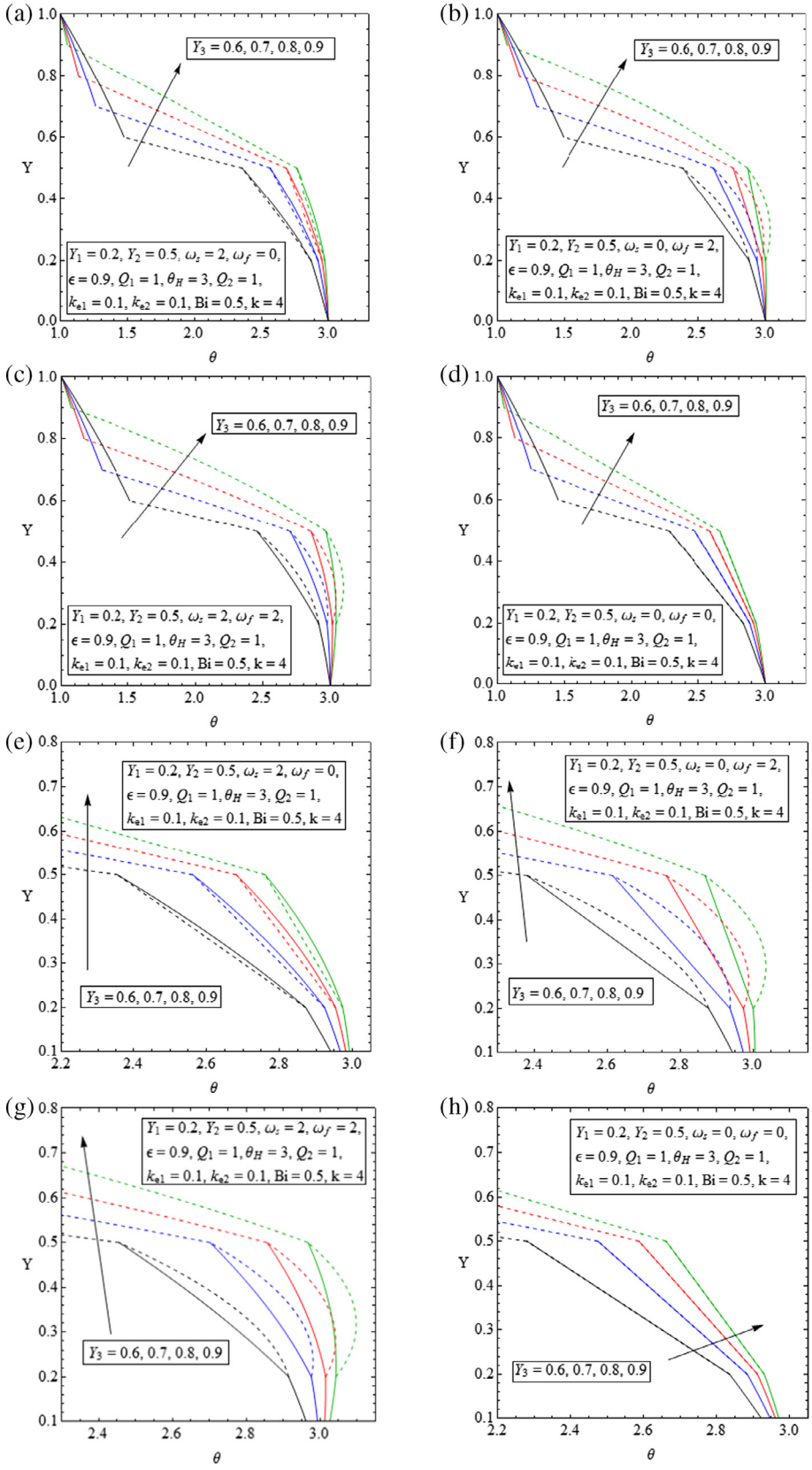

Fig. 5. Temperature distribution with various values of the upper wall thickness, Y_3 (a–d) and focussing on the porous region (e–h), (a & e) Case 1, (b & f) Case 2, (c & g) Case 3, and (d & h) Case 4.

Fig. 5a and e, corresponding to the changes in the thickness of the upper wall.

Moving to case 2, investigated in parts b and f of Figs. 3–5, results in a substantial temperature difference in the porous region, which persists under all configurational variations. Compared with case 1, temperature difference between the two phases in the porous medium of the system in case 2, has greatly increased (see Figs. 3f, 4f and 5f). In all of the investigated cases, having ninefold more fluid phase within the porous insert compared to that of the solid phase, i.e. $\epsilon = 0.9$, may be an important reason for the major quantitative differences between the temperature fields within the porous medium of cases 1 and 2. However, as intuitively can be perceived, the inclusion of the source term in the solid phase of the porous media, i.e. case 1, increases the temperature of the solid phase compared to that of the fluid phase. Similarly, the fluid phase temperature of the porous medium in case 2 is higher than the temperature of the solid phase. In a qualitative agreement with that discussed for case 1, increasing the thicknesses of the lower wall and the porous insert tends to reduce the temperature difference between the two phases in the porous part of the system. This behaviour is almost repeated in Figs. 3c–5c (and correspondingly in Figs. 3g–5g), in which equal exothermicity applies to the solid and fluid phases (case 3). The local equilibrium trend observed here is generally in keeping with that discussed in partially-filled porous channels with exothermicity [23,24]. Nevertheless, inclusion of the thick walls in the present problem makes the thermal behaviour of system more complicated. For instance, Fig. 3 implies that variations in the thickness of the lower walls do not affect the temperature of the upper wall. Yet, modifying the thickness of the porous layer (Fig. 4) and that of the upper wall (Fig. 5) can change the temperature of the entire system noticeably.

The preceding analysis indicates that the strength of internal heat generations is an important parameter influencing the thermal characteristics of the system. This is further investigated in Fig. 6a–d through varying the thermal energy source terms within the fluid and solid phases for two different values of porosity. The range of this variation includes negative values of the source terms, which refers to endothermic chemical reactions (such as those encountered in reforming processes [17]). Fig. 6a and b show that variation in the internal heat sources within the fluid phase can majorly modify the temperature profiles across the system. Further, the temperature difference between the fluid and solid phases in the porous region is strongly affected by this parameter [23,24]. Larger values of internal heat generation in the fluid temperature signify the temperature difference and push the system towards LTNE. These arguments equally apply to Fig. 6c and d, in which internal heat generation is limited to the solid phase of the porous medium. As an important difference, however, heat generation in the solid phase appears to be less capable of disturbing the local

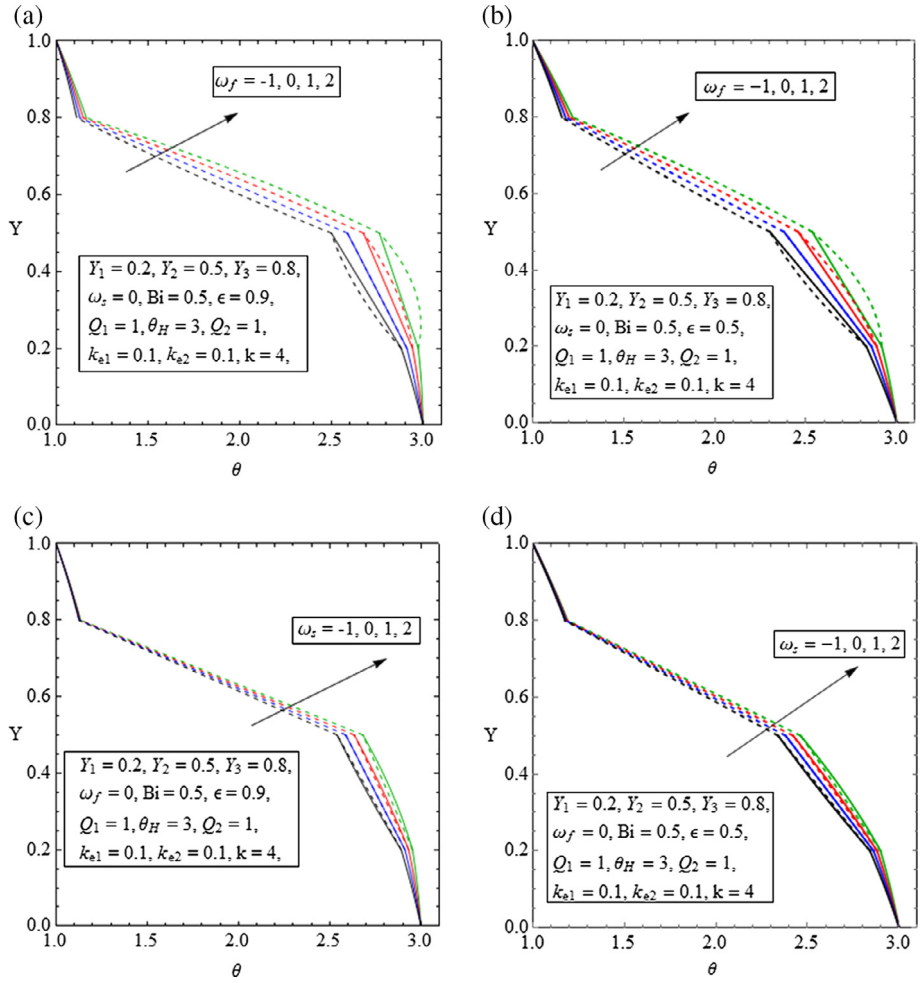

Fig. 6. Temperature distribution with different values of exothermicity and endothermicity (a) in the porous fluid phase, ω_f for porosity, $\varepsilon = 0.9$, (b) in the porous fluid phase, ω_f for porosity, $\varepsilon = 0.5$, (c) in the porous solid phase, ω_s for porosity, $\varepsilon = 0.9$, and (d) in the porous solid phase, ω_s for porosity, $\varepsilon = 0.5$.

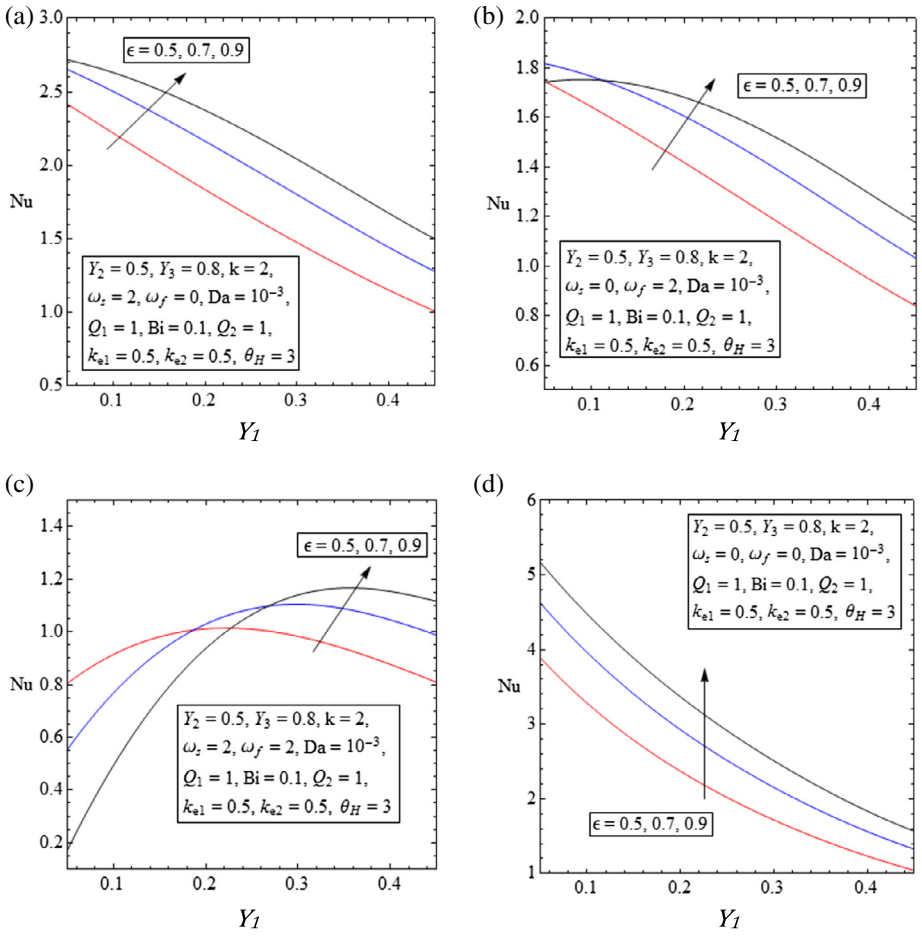

Fig. 7. Variation in *Nu* versus the lower wall thickness, Y_1, for different values of porosity. (a) Case 1, (b) Case 2, (c) Case 3, and (d) Case 4.

thermal equilibrium of the system. It is important to note that variations in the porosity of the insert in Fig. 6b and d does not change this argument.

3.2. Nusselt number

Section 3.1 showed that the geometrical configuration of the microreactor can significantly affect the temperature distributions. This implies that the rates of heat transfer and therefore the *Nu* (as defined in Eq. (14)) would change by varying the system configuration. Figs. 7–9 illustrate such modifications of *Nu*. Fig. 7 depicts the values of *Nu*, for the four cases of Table 1. In this figure *Nu* has been calculated for a few different values of porosity. A comparison of Fig. 7a–d reveals that variation in the exothermicity in cases 1–4 causes significant qualitative and quantitative changes in the behaviour of the *Nu*. In the basic case with no exothermicity (case 4 shown in Figs. 7d and 8d) the behaviour of *Nu* is monotonic with respect to increase in the thickness of the lower wall and increasing porosity of the porous insert. In Fig. 7d, *Nu* has a value between 4 and 5 for the thin wall system and its magnitude decreases sharply by thickening the lower wall. Introduction of exothermicity in Fig. 7a–c results in a general decrease in the numerical value of the *Nu*. This observation is consistent with the fact that for cases 1–3 the average temperature across the channel, shown in Fig. 3, is higher than that of case 4. Lower heat transfer coefficients in the internally heat generating cases leads to higher temperatures in the system and therefore larger heat transfer potentials. Further, Fig. 7b and c show that in cases 2 and 3 there exist optimal values of the lower wall thickness, which render maximum *Nu*. Fig. 10c indicates that the optimal thickness increases with increasing the porosity. It follows that in microreactors with exothermic fluids the thickness of the wall can play a significant role in heat transfer characteristics of the system. For example, as it can be clearly seen from Fig. 7b, for $\epsilon = 0.9$, the *Nu* is maximised when the lower wall thickness is close to $Y_1 = 0.15$. This is particularly important as the current analysis shows that introduction of exothermicity in the fluid can generally bring down the *Nu* in comparison with the corresponding system with no exothermicity. Hence, selecting the right wall thickness becomes an essential task in the thermal design of microreactors with highly exothermic reactions.

It is, generally, known that the thickness of the porous insert in the partially-filled conduits is an essential parameter dominating the rate of heat transfer [28,29]. Fig. 8 shows that thick wall microchannels with exothermic chemical reactions can further substantiate the role of porous insert thickness. In Fig. 8a (case 1), starting from a relatively thin porous insert ($Y_2 = 0.2$) and increasing the thickness of the porous layer can signify the value of *Nu*. This is more pronounced at higher values of porosity. Fig. 8a shows that for small thicknesses of the porous insert, first there is a *Nu* decreasing trend, which continues till a minimum value is reached. The exact value of this minimum *Nu* depends upon the configurational parameters such as porosity. Nonetheless, Fig. 8a indicates that while making the insert more porous can generally increase the *Nu*, the location of the minimum point remains more and less insensitive to this parameter. Fig. 8b shows that addition of exothermicity to the fluid (case 2) alters the situation noticeably. Here, for the small thicknesses of the porous insert

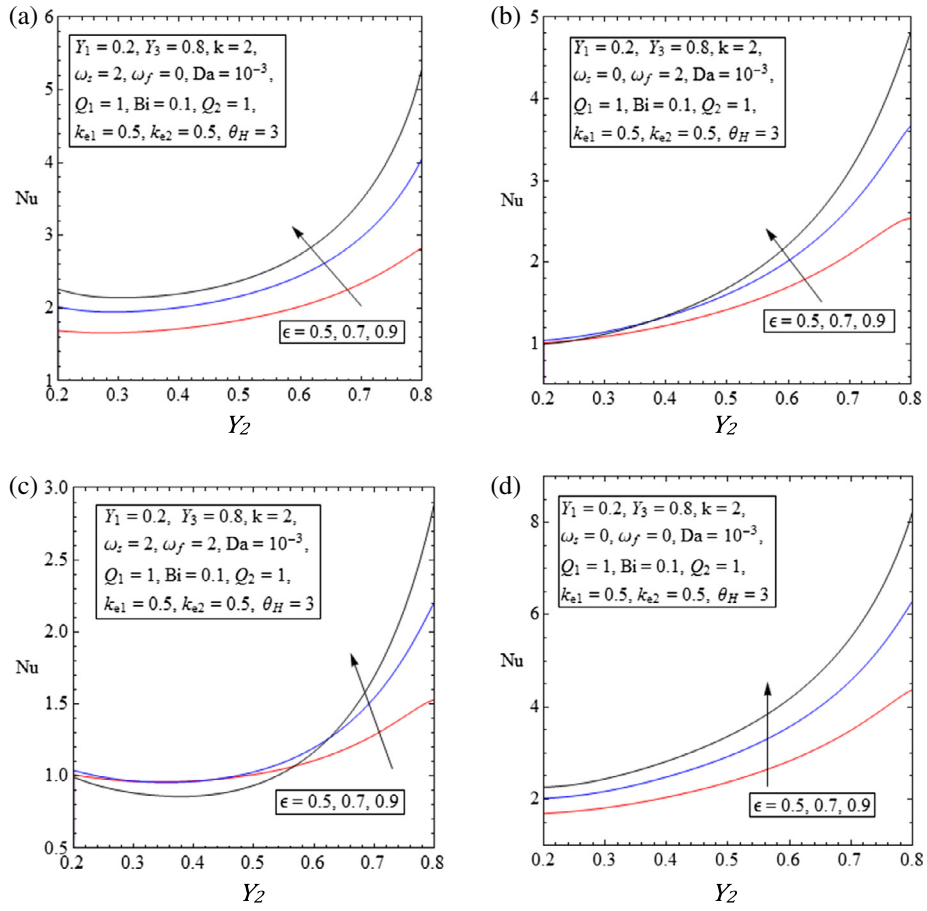

Fig. 8. Variation in *Nu* versus the porous insert thickness, Y_2, for different values of porosity. (a) Case 1, (b) Case 2, (c) Case 3, and (d) Case 4.

Nu number is almost independent of the porosity. Further increase in the thickness of the porous insert results in increasing the value of *Nu*, while the rate of increase appears to be greater at higher porosities. Considering exothermicity in both solid and fluid (case 3 shown in Fig. 8b) complicates the behaviour of *Nu*. Similar to that discussed for case 1 (Fig. 8a) increasing the thickness of the porous insert in case 3 first results in the reduction of the *Nu* number and development of minima in Fig. 8c. This is particularly noticeable for the highest value of porosity. Once again, the location of these minima are not strongly affected by the changes in porosity. Further thickening the porous insert substantiates the value of *Nu*. Nonetheless, comparing to Fig. 8a and b for a given thickness of the porous insert the numerical value of *Nu* in Fig. 8c is considerably lower. Removing all sources of exothermicity in Fig. 8d (case 4) greatly simplifies the problem. Here, for all investigated porosities, the *Nu* increases monotonically with increases in the thickness of the porous insert. Importantly, the numerical values of *Nu* number in Fig. 8d are higher than all other cases, revealing the adverse effect of exothermicity on the heat convection process. These significant modifications through addition of exothermicity clearly reflect the importance of considering the exothermic terms under an LTNE framework.

Fig. 9 illustrates the effects of changes in the thickness of the upper wall of Fig. 1 on the *Nu*. The general trend observed in this figure is somehow similar to that of Fig. 7, in which the value of *Nu* is often correlated with the porosity and wall thickness. However, like the lower wall effects shown in Fig. 7, thickening of the upper wall results in a monotonic decrease of the *Nu*. An exception to this is case 3 (Fig. 9c), in which at the highest investigated porosity the *Nu* variation versus the wall thickness features a maximum point. Figs. 7–9 clearly show that in the absence of internal heat generation the heat transfer behaviour of the microchannel shown in Fig. 1 is fairly simple. However, inclusion of exothermicity in the system can introduce major complexities. As such the changes of *Nu* with respect to change in the thickness of the system components is not monotonic anymore and can feature extremum points. Further, the existence of exothermic sources in the microchannel can signify the sensitivity of the heat transfer processes to the porosity of the porous insert and cause a general reduction in the value of *Nu*. Clearly, these findings have direct consequences upon the design and operation of microreactors.

The microchannel configuration under investigation (Fig. 1) can include internal heat generations within the thick walls of the system. As discussed earlier, this is a manifestation of the absorption of microwaves or infrared waves by the solid structure of the microreactor. Although not shown here, there appeared to be a general positive correlation between the *Nu* and wall internal heat generation. Further, in keeping with the results shown in other figures, high values of porosity produce larger *Nus*. The relation between *Nu* and the porosity of the porous layer is further investigated in Fig. 10a. This figure shows changes of the *Nu* against porosity for varying values of the lower wall internal heat generation. Evidently, Fig. 10a features an extremum behaviour and reflects initial increase of the *Nu* with increasing the porosity followed by a sudden drop. Interestingly, variation of the intensity of heat generation in the wall appears to have a relatively small effect on the optimal porosity and the maximum *Nu*. The effects of exothermicity and endothermicity within the fluid and porous solid phase upon the *Nu* are investigated in Fig. 10b and c. It is clear from these figures that reduction of the endothermicity and

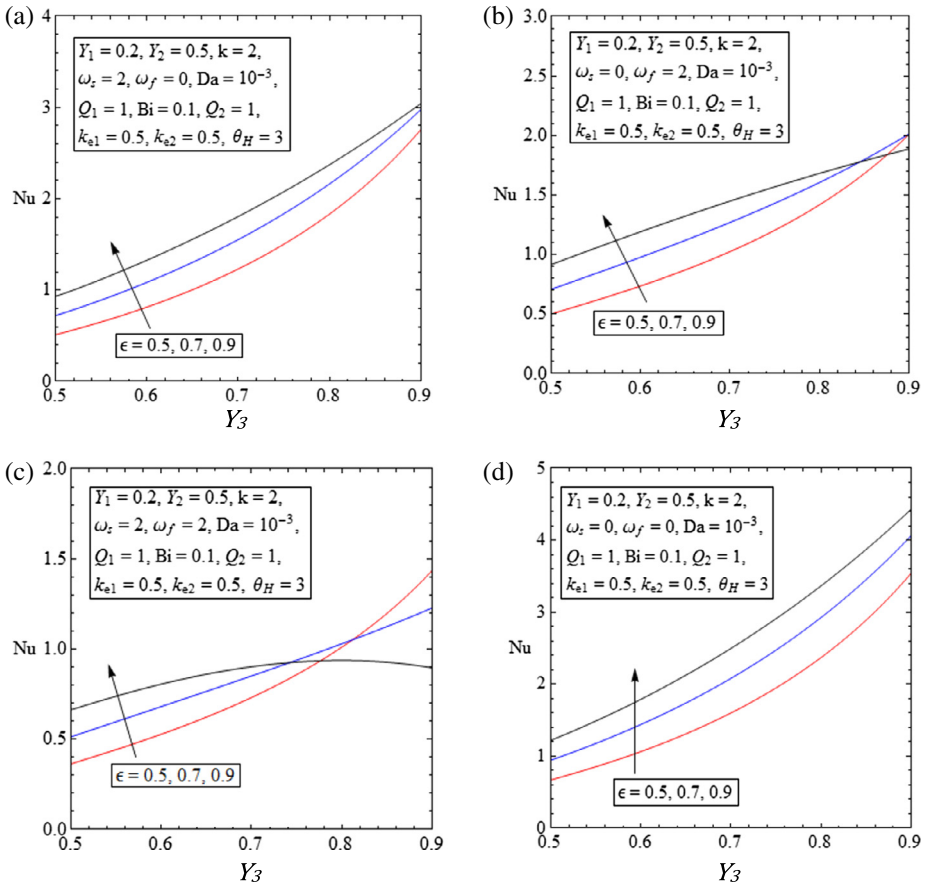

Fig. 9. Variation in *Nu* versus the upper wall thickness, Y_3, for different values of porosity. (a) Case 1, (b) Case 2, (c) Case 3, and (d) Case 4.

increases in the exothermicity in either of the fluid and porous solid phase results in decreasing the *Nu*. For a similar range of internal heat generation in Fig. 10b and c, the *Nu* drop in Fig. 10b is more significant. This implies that compared to that of porous solid, the fluid exothermicity/endothermicity has a stronger effect upon the *Nu*. Further, Fig. 10b and c both show that as the magnitude of exothermicity increases the influences of porosity on the value of *Nu* decreases. This trend is particularly clear in Fig. 10c. A comparison between Fig. 10b and c further reveals that the numerical value of *Nu* varies significantly by shifting the internal heat source from the fluid to the solid phase. This is yet another factor emphasising the importance of considering LTNE approach in the thermal analysis of microreactors.

3.3. Entropy generation

3.3.1. Local entropy generation

The effects of configurational variations on the local generation of entropy across the microchannel has been analysed in Figs. 11–13. Fig. 11 shows the modification of local entropy generation caused by the changes in the thickness of the porous layer. The four cases of Table 1 have been investigated in this figure. As a general trend in Fig. 11, it is observed that for all cases the generation of entropy increases by thickening the porous layer. This increase can be seen in all components of the system (the solid walls, solid and fluid phase within the porous region and the fluid phase in the clear region). Nonetheless, it appears that the fluid in the clear region and the solid upper wall are most affected by the variations in the thickness of the porous layer. Comparing to case 1, the extent of these changes seem to be slightly larger in cases 2 and 3, while case 1 features the lowest local entropy generation. This is consistent with the observations made in similar configurations with zero wall thickness [23,24] and hence, is not further discussed. As stated earlier, the finite thickness of the microchannel walls is a distinctive feature in the thermal analysis of microreactors. The effects of variations in this parameter upon the local entropy generation have been depicted in Fig. 12. This figure shows that, for all cases under investigation, altering the thickness of the upper wall of the microchannel, which is directly related to that of the clear section of the microchannel, noticeably affects the local entropy generation. It is clear from this figure that increasing the thickness of the upper wall of the channel signifies an increase in the local generation of entropy. This may be partially due to the fact that the thermal conductivity of the wall is much higher than that of the fluid material, and therefore increasing the thickness of the upper wall increases the rate of heat transfer, and consequently the local entropy generation rate is enhanced. Similar to that discussed in Fig. 11, the extent of this increase is minimal in case 4 (shown in Fig. 12g) and maximum in case 3 (Fig. 12e). However, the situation is different in the porous region, in which case 2 shows the minimum local entropy generation (Fig. 12d) and cases 1 and 4 (Fig. 12b and h) are the most irreversible cases.

The thermal asymmetry due to the exposure of the system to two different temperatures at the outer most boundaries is expected to be a strong source of irreversibility. This thermal asymmetry is very common in microreactors and particularly can be found in reforming applications, in which sustaining the process is often subject to asymmetric transfer of heat [7,53]. Fig. 13 shows how changes in the ratio of the outer surface temperatures, θ_H, affects the local generation of entropy. According to this figure,

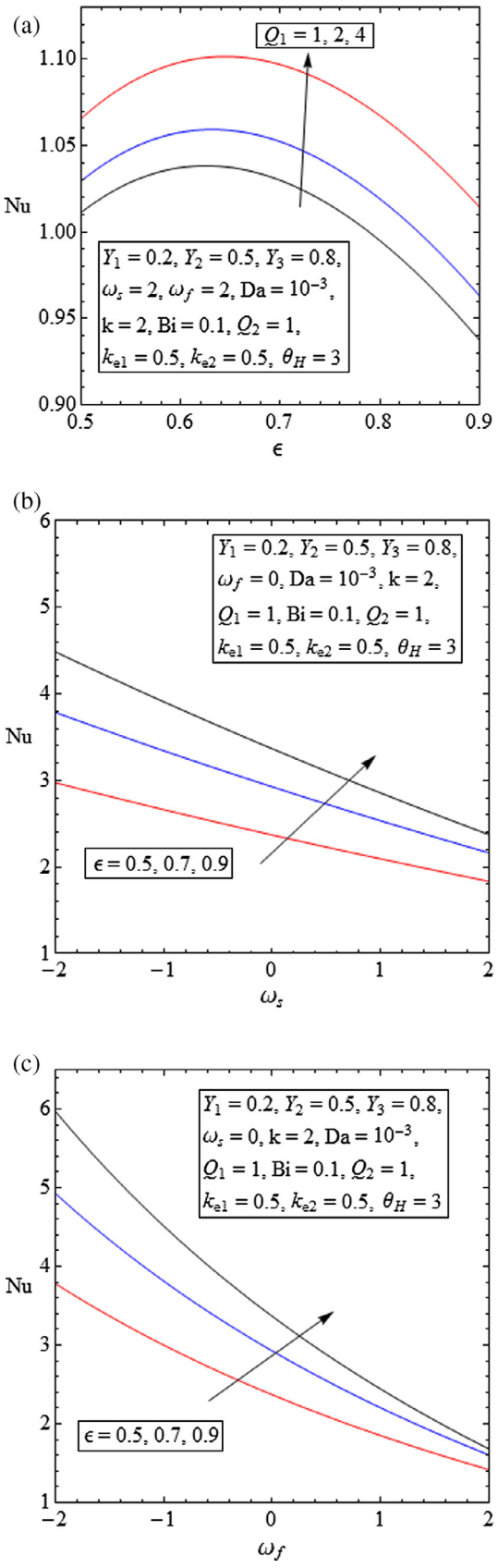

Fig. 10. Variation in *Nu* versus (a) porosity, ε, for different values of heat generation in the lower wall, Q_1 for Case 3, (b) heat source/sink in the porous solid phase, ω_s, for different values of porosity, and (c) heat source/sink in the fluid phase, ω_f, for varying values of porosity.

entropy generation can be intensified by an order of magnitude with a modest change in θ_H between 1.5 and 5. Importantly, Fig. 13 indicates that variations in θ_H can strongly affect the generation of entropy within the clear region of the microchannel and the upper wall. The existence of exothermic sources in the system (cases 1–3 shown in Fig. 13a, c and e) appear to signify this irreversibility. Given that in reality microreactors used for reforming can be exposed to catalytic combustion on one side and room temperature on other side, the value of θ_H is expected to be between 3 and 4 [7]. Fig. 13 shows that at these values of θ_H the irreversibility caused by the thermal asymmetry of the system is quite significant and should be certainly included in any second law analysis of the microreactor.

Intuitively, the exothermicity of microreactor, represented by the internal heat generations within the solid and fluid phases, could be a major source of entropy production. Fig. 14 implies that although the general notion of generation of entropy by exothermicity/endothermicity is correct, this factor is not as significant as other investigated parameters. Fig. 14e shows that, compared to a case with no internal heat generation, addition of relatively strong thermal energy source terms ($\omega_f = \omega_s = 2, -2$) alters the local entropy generation by less than 40%. A similar behaviour is observed in Fig. 14a and c, in which internal heat generation is respectively limited to the fluid and porous solid phase. This figure, further, shows that variation in the internal energy generation within the fluid and solid phases leads to a common intersection of entropy generation curves in the clear fluid region. This bifurcation behaviour is a characteristic of fluid conduits with internal heat generations and has been recently studied in Refs. [23,24]. The common intersections are also present inside the porous region, (Fig. 14b, d and f). They occur in the fluid phase for cases with internal heat generations in the fluid only (Fig. 14b) and equal thermal energy source term in the solid and fluid (Fig. 14f), and within the solid region when heat is exclusively generated inside the porous solid (Fig. 14d).

3.3.2. Total entropy generation

Integration of the local entropy generation over the entire volume of the system (as in Eq. (17)) results in the calculation of the total entropy generation. In general, this leads to the development of an analytical, multivariable function. The resultant total entropy function can be then differentiated revealing the local minima and maxima. In the current work, however, the total entropy function is overwhelmingly complicated and large. Analytical differentiation of such function is practically unfeasible and hence numerical analyses are conducted instead (see Section 2) to explore the behaviour of the total entropy. Although not shown here, a parametric study of the total entropy generation revealed that for all investigated cases in Table 1, increasing the porosity of the porous insert results in a considerable reduction of the total entropy. This appears to be true for all variations in the system geometrical configurations and also changes in the thermal asymmetry of the system. The results discussed in Sections 3.1 and 3.2 showed that the thickness of the upper wall is an important parameter influencing the temperature profiles and *Nu*. It was, further, shown in Section 3.3.1 that the wall thickness strongly affects the local generation of entropy. In Fig. 15a the total entropy production, N_t, has been plotted against the thickness of the porous layer, Y_2 (for constant value of Y_1) in this figure the variations of N_t versus Y_2 has been demonstrated for different values of the upper wall thickness (Y_3). This figure indicate that for a modestly thick upper wall ($Y_3 = 0.9$) there are two extremum points for the variations of the total entropy generation with the porous layer thickness. The first extremum point is a local maximum and occurs

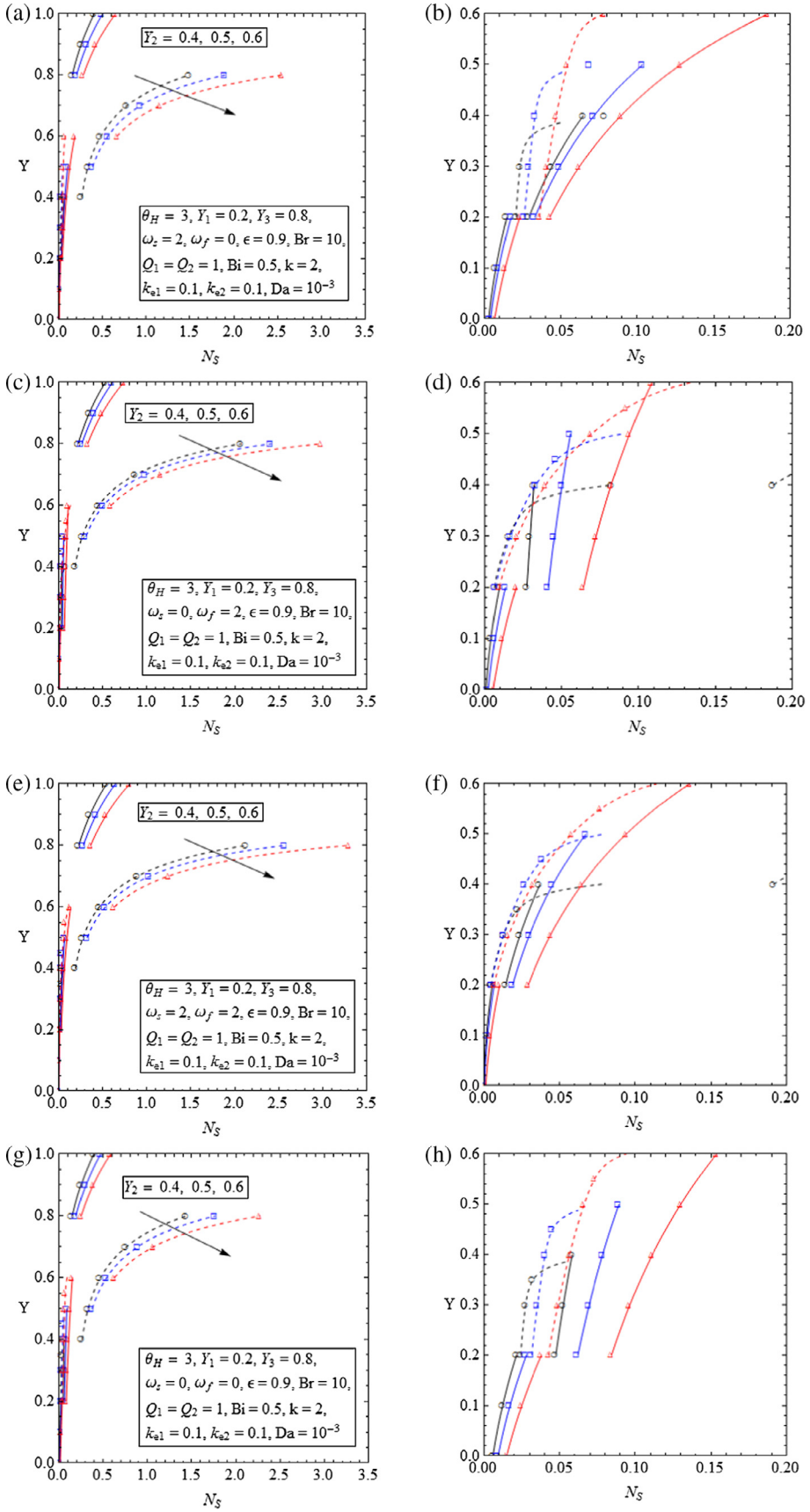

Fig. 11. Local entropy generation distribution with various values of the porous insert thickness, Y_2. Full graphs on left and graphs focussing on porous region on the right. (a & b) Case 1, (c & d) Case 2, (e & f) Case 3, (g & h) Case 4.

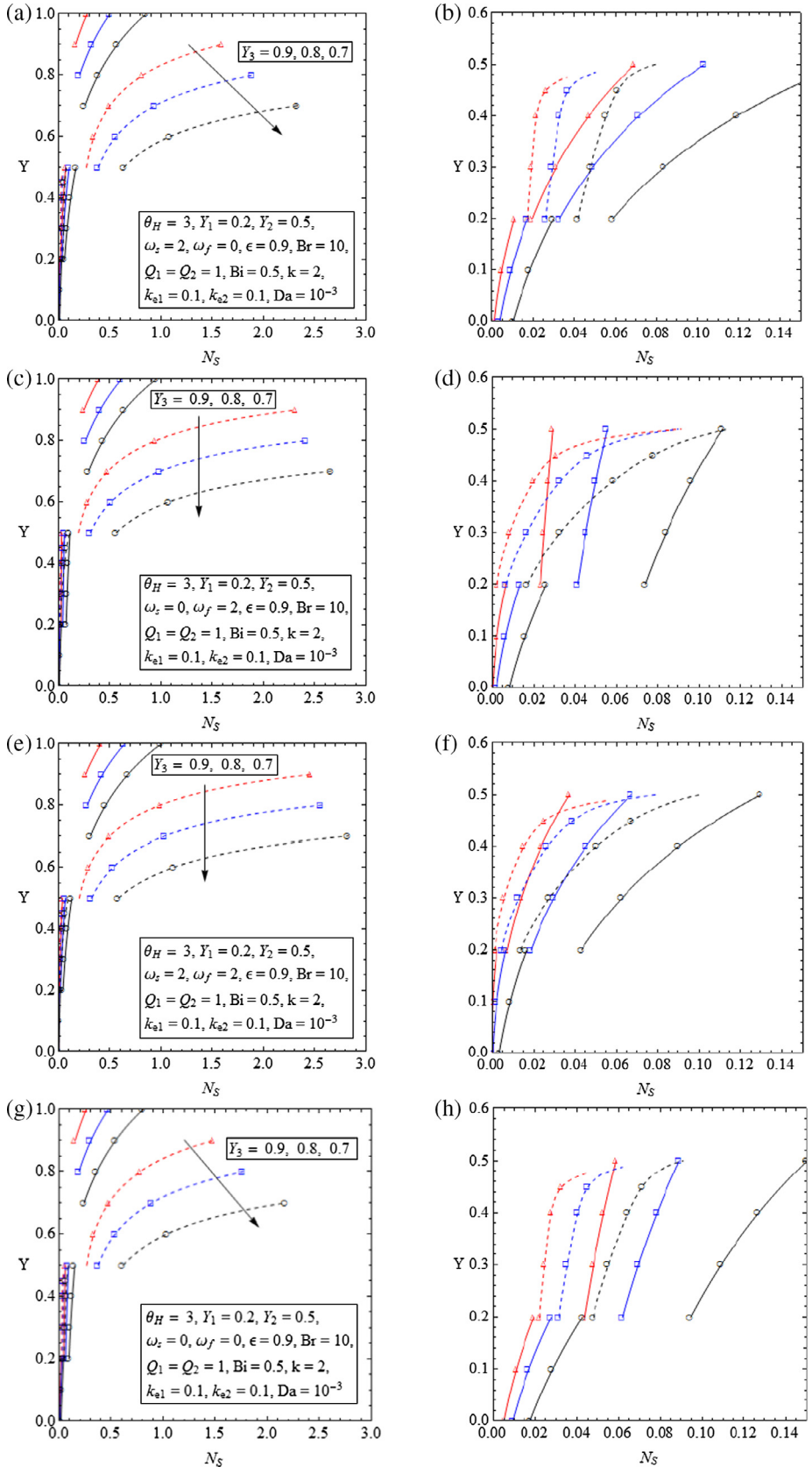

Fig. 12. Local entropy generation distribution with various values of the upper wall thickness, Y_3. Full graphs on left and graphs focussing on porous region on the right. (a & b) Case 1, (c & d) Case 2, (e & f) Case 3, (g & h) Case 4.

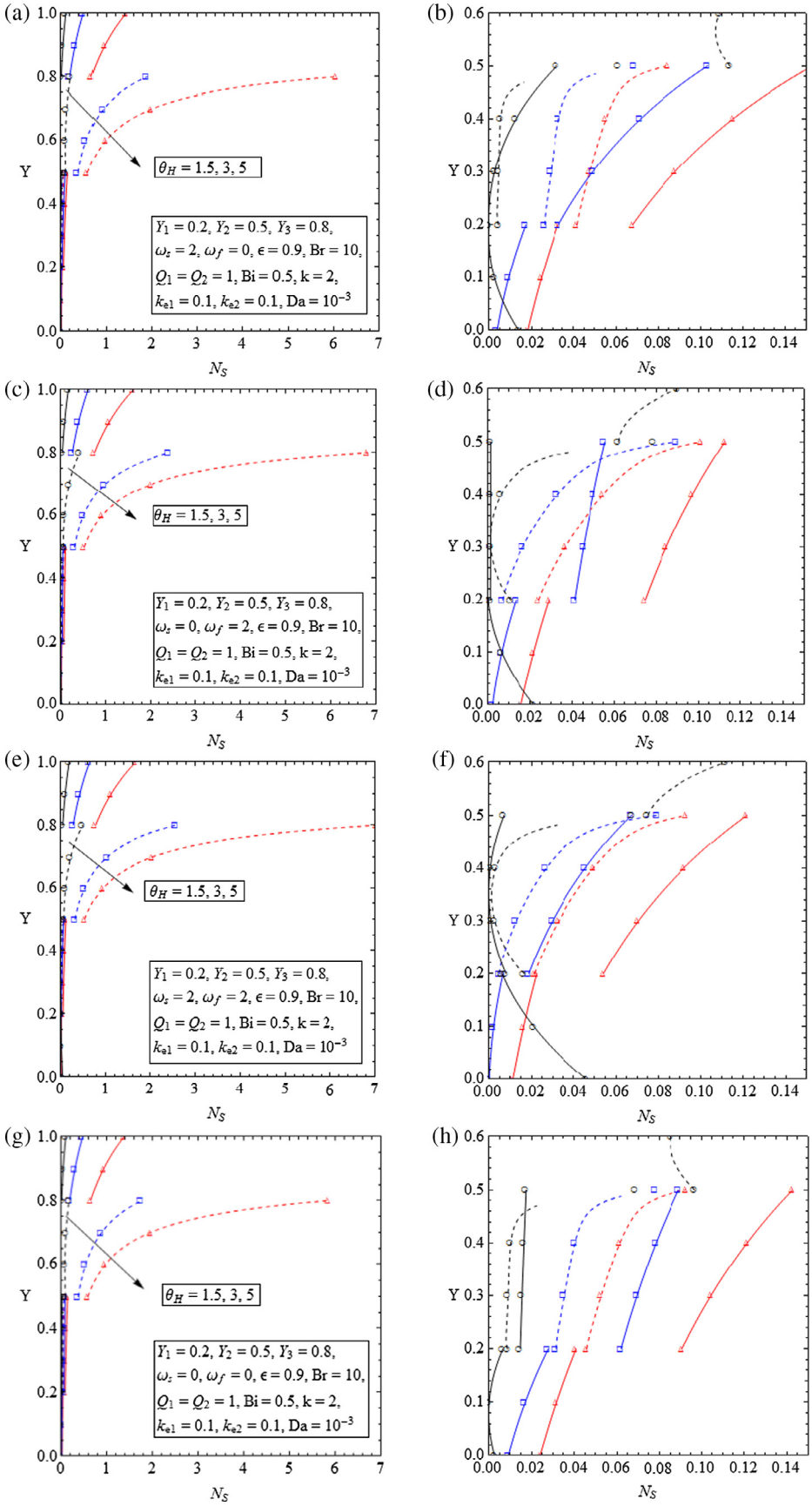

Fig. 13. Local entropy generation distribution with various values of the lower wall temperature, θ_H. Full graphs on left and graphs focussing on porous region on the right. (a & b) Case 1, (c & d) Case 2, (e & f) Case 3, (g & h) Case 4.

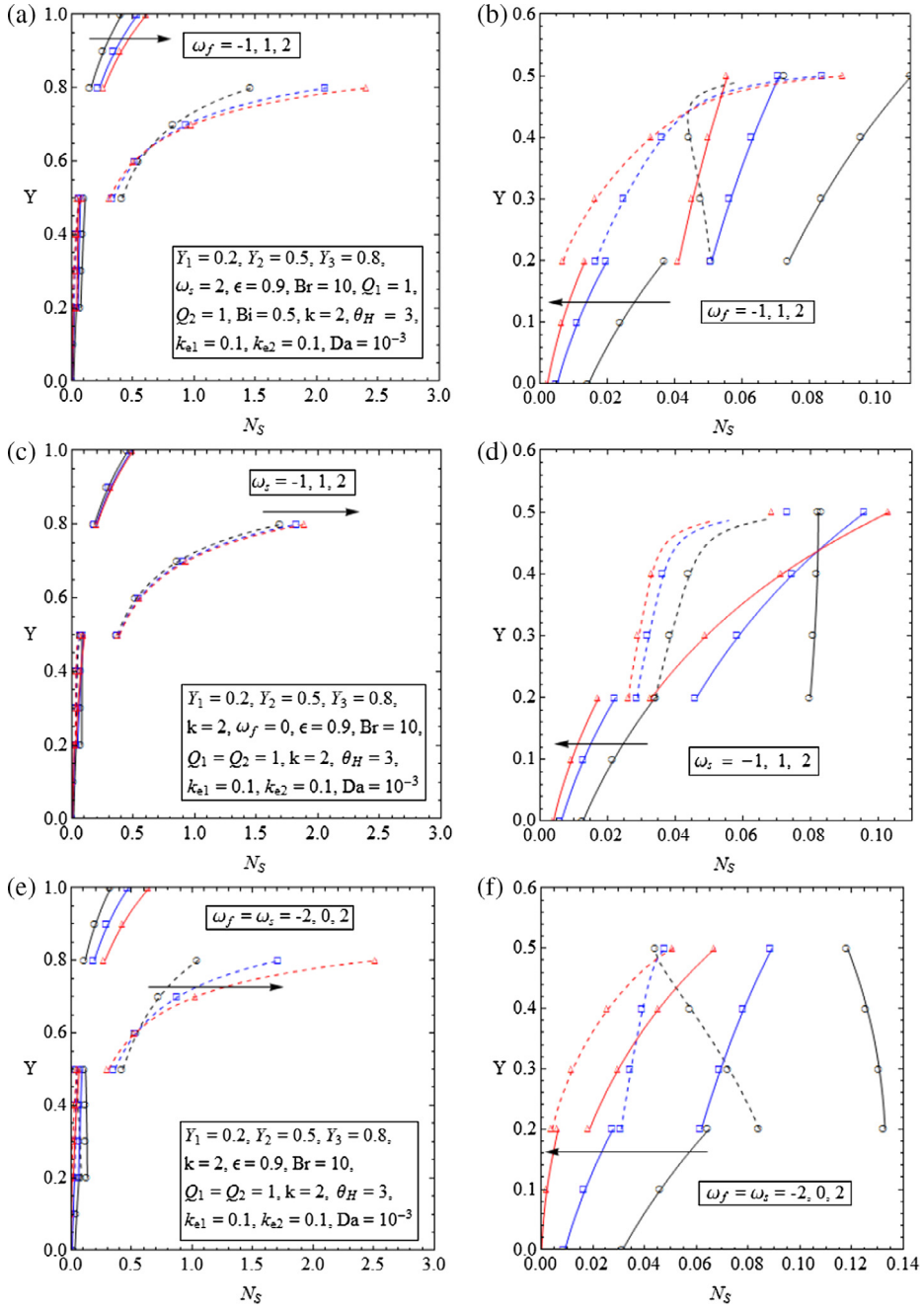

Fig. 14. (a & b) Local entropy generation distribution for different values of ω_f and no heat source/sink in the solid porous phase. (c & d) Local entropy distribution for different values of ω_s and no heat source/sink in the fluid phase. (e & f) Local entropy distribution for different values of ω_f and ω_s. Full graphs on left and graphs focussing on porous region on the right.

at thin porous thicknesses. As the porous layer grows in thickness a second extremum point appears in the form of a local minimum. Further increase in the thickness of the porous insert results in a monotonic growth in the total entropy generation. Alteration of the system configuration towards very thin upper walls ($Y_3 = 0.95$) shifts the location of the minimum point towards higher thicknesses of the porous insert. A qualitatively similar behaviour is observed in Fig. 15b, in which N_t has been plotted versus Y_2 for different values of the lower wall thickness. Interestingly, smaller values of the lower wall thickness in Fig. 15b have similar effects as low thicknesses of the upper wall in Fig. 15a.

It was observed in Sections 3.2 and 3.3.1 that the thermal asymmetry of the system has a very strong effect upon the temperature fields, heat transfer and local entropy generation of the microreactor. Fig. 15c shows that the pronounced influences of this parameter are readily extended to the total entropy generation. This figure depicts the variation of the total entropy versus thickness of the porous layer for three different values of the outer surfaces temperature ratio θ_H. The existence of a minimum entropy point is evident in Fig. 15c, in which for larger values of θ_H the minimum entropy occurs at smaller thicknesses of the porous insert. This behaviour can have direct consequences on the exergetic design

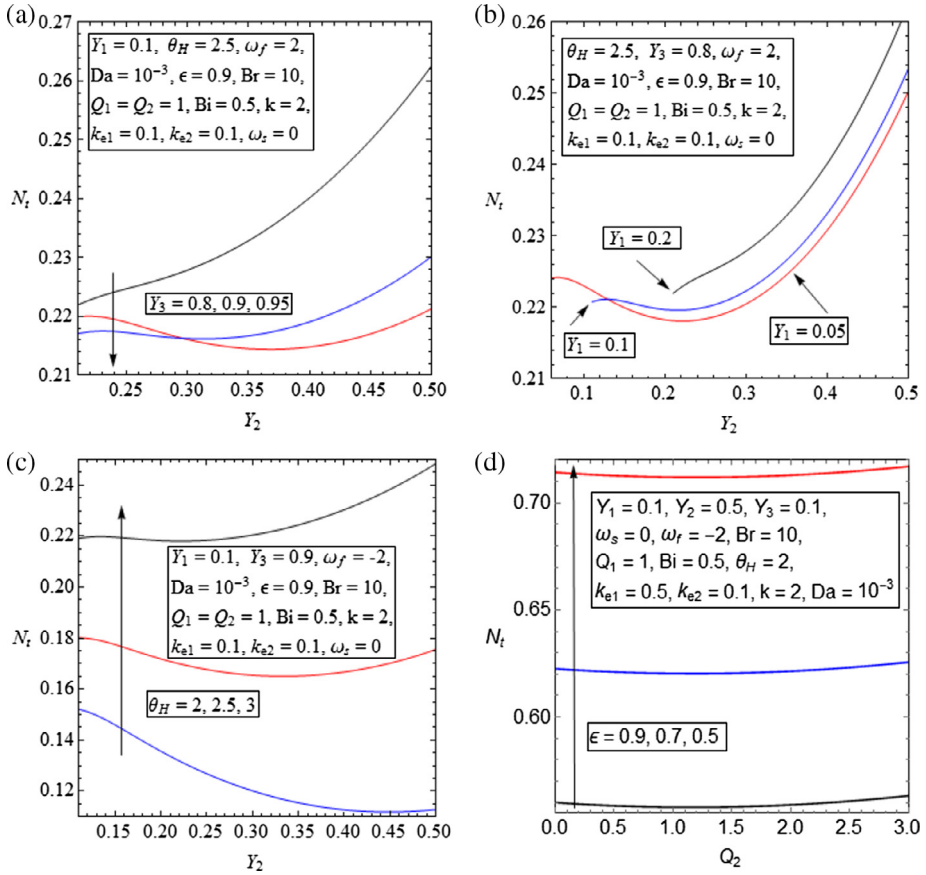

Fig. 15. Total entropy versus (a) porous insert thickness, Y_2 for various values of the upper wall thickness, Y_3, (b) porous insert thickness, Y_2 for various values of the lower wall thickness, Y_1, (c) the porous insert thickness, Y_2, for different values of the lower wall temperature, θ_H, (d) heat source/sink in the upper wall, Q_2 for different values of porosity under conditions of a heat sink in the fluid phase and walls of thickness 0.1.

of the microreactor. It implies that for any value of θ_H there is an optimal thickness of the porous insert, which results in the minimisation of the total entropy generation in the system.

Fig. 15d illustrates the effects of internal heat generation inside the wall on the total entropy generation. In this figure, the total entropy has been plotted for different values of porosity. Although changes of the total entropy generation with the increases in the wall internal heat generation are relatively small, there exist a minimum point in each graph of Fig. 15d. Further, the numerical value of entropy production appears to be strongly dependent on the porosity and takes a higher value at lower porosities. However, the optimal non-dimensional heat generation in the wall is almost insensitive to the porosity. This is such that for all investigated porosities the optimal internal heat generation in the upper wall is around $Q_2 = 1.2$. Finally, it is noted that there exists a monotonic and positive relation between the total entropy generation and rates of exothermicity and endothermicity within the fluid and porous solid. Nonetheless, for brevity reasons, the corresponding figure is not shown here.

In closing, it is worth nothing that the findings of this study should be implemented most carefully. The heat transfer analyses of the problem showed that there is a strong connection between the exothermicity and wall thicknesses and the optimal Nusselt number. The same applies to the total entropy generation. Similar to other engineering devices, in microreactors the optimal configurations for the Nusselt number and minimum entropy generation are not necessarily identical. Nonetheless, the investigations discussed in this section revealed that the changes in the Nusselt number and the total entropy generation are qualitatively consistent. Thus, the final decision should be made by the designer to consider which aspect of the thermal design of the microreactor more important to the particular problem at hand.

4. Conclusions

A thermal model was established for microreactors accommodating highly exothermic/endothermic reactions. This includes a thick wall, asymmetric microchannel partially-filled with a porous material subject to constant but unequal temperatures at the outermost surfaces. The heat of reactions and absorption of microwaves and infrared waves were represented by volumetrically uniform, energy source terms. The porous region was assumed under local thermal non-equilibrium. It was argued that in such system the irreversibility is dominated by the thermal effects and hence mass transfer and chemical irreversibilities were ignored. In the limit of low thermal Peclet number, analytical solutions were developed for the conjugate heat transfer problem as well as the local and total entropy generations. A comprehensive parametric study was subsequently conducted. The major findings of this study can be summarised as follows.

- Introduction of the heat of reaction and internal heat generations can significantly perturb the system from LTE condition. The extent of this deviation depends on the configuration of the microreactor. In particular, the thickness of the porous insert was found to be a dominating factor. This finding substantiates the necessity of applying LTNE in the thermal analysis of microreactors.

- It was shown that the variations in the thicknesses of the walls and porous insert in the microreactor can majorly modify the *Nu*. This is such that by varying these parameters some extremum points appear in the *Nu* graphs, indicating the existence of optimum configurations.
- *Nu* appeared to be inversely correlated with the internal heat generations, whilst demonstrating a positive correlation with the porosity of the insert.
- Changes in the wall and porous layer thickness led to the formation of minimum total entropy generation points.
- Thermal asymmetry of the system appeared to be an important source of irreversibility and its variation could minimise the total entropy production.

These points clearly reflect the significant role of the microstructure in shaping the thermal and entropic behaviour of microreactors. It further shows that to achieve an optimal design, thermal characteristics of the system such as thermal boundary conditions and internal heat generation should be considered in conjunction of the configurational specification of the system.

Acknowledgement

The financial support of the University of Glasgow through EPSRC DTA (G. Hunt) EPSRC funding award number EP/M506539/1 is gratefully acknowledged.

References

[1] J. Stolte, L. Özkan, P.C. Thüne, J.W. Niemantsverdriet, A.C.P.M. Backx, Pulsed activation in heterogeneous catalysis, Appl. Therm. Eng. 57 (2013) 180–187, http://dx.doi.org/10.1016/j.applthermaleng.2012.06.035.
[2] G. Kolb, V. Hessel, Micro-structured reactors for gas phase reactions, Chem. Eng. J. 98 (2004) 1–38, http://dx.doi.org/10.1016/j.cej.2003.10.005.
[3] T. Wirth, Microreactors in Organic Chemistry and Catalysis, 2013, 470.
[4] E.V. Rebrov, J.C. Schouten, M.H.J.M. de Croon, Single-phase fluid flow distribution and heat transfer in microstructured reactors, Chem. Eng. Sci. 66 (2011) 1374–1393, http://dx.doi.org/10.1016/j.ces.2010.05.044.
[5] R. Guettel, T. Turek, Assessment of micro-structured fixed-bed reactors for highly exothermic gas-phase reactions, Chem. Eng. Sci. 65 (2010) 1644–1654, http://dx.doi.org/10.1016/j.ces.2009.11.002.
[6] V. Kumar, M. Paraschivoiu, K.D.P. Nigam, Single-phase fluid flow and mixing in microchannels, Chem. Eng. Sci. 66 (2011) 1329–1373, http://dx.doi.org/10.1016/j.ces.2010.08.016.
[7] N.S. Kaisare, D.G. Vlachos, A review on microcombustion: fundamentals, devices and applications, Prog. Energy Combust. Sci. 38 (2012) 321–359, http://dx.doi.org/10.1016/j.pecs.2012.01.001.
[8] Y. Lei, W. Chen, J. Lei, Combustion and direct energy conversion inside a microcombustor, Appl. Therm. Eng. 100 (2016) 348–355, http://dx.doi.org/10.1016/j.applthermaleng.2016.01.162.
[9] M.-T. Lee, C.P. Grigoropoulos, R. Greif, A study of the transport phenomena in a wall-coated micro steam-methanol reformer, Int. J. Hydrogen Energy 39 (2014) 2008–2017, http://dx.doi.org/10.1016/j.ijhydene.2013.11.107.
[10] M.J. Stutz, D. Poulikakos, Effects of microreactor wall heat conduction on the reforming process of methane, Chem. Eng. Sci. 60 (2005) 6983–6997, http://dx.doi.org/10.1016/j.ces.2005.06.012.
[11] T. Illg, P. Löb, V. Hessel, Flow chemistry using milli- and microstructured reactors-from conventional to novel process windows, Bioorg. Med. Chem. 18 (2010) 3707–3719, http://dx.doi.org/10.1016/j.bmc.2010.03.073.
[12] X. Yao, Y. Zhang, L. Du, J. Liu, J. Yao, Review of the applications of microreactors, Renew. Sust. Energy Rev. 47 (2015) 519–539, http://dx.doi.org/10.1016/j.rser.2015.03.078.
[13] V. Hessel, A. Renken, J.C. Schouten, J.-I. Yoshida (Eds.), Micro Process Engineering, Wiley-VCH Verlag GmbH & Co. KGaA, Weinheim, Germany, 2009, http://dx.doi.org/10.1002/9783527631445.
[14] S.-X. Zhang, Y.-L. He, G. Lauriat, W.-Q. Tao, Numerical studies of simultaneously developing laminar flow and heat transfer in microtubes with thick wall and constant outside wall temperature, Int. J. Heat Mass Transfer 53 (2010) 3977–3989, http://dx.doi.org/10.1016/j.ijheatmasstransfer.2010.05.017.
[15] M. Torabi, G.P. Peterson, Effects of velocity slip and temperature jump on the heat transfer and entropy generation in micro porous channels under magnetic field, Int. J. Heat Mass Transfer 102 (2016) 585–595, http://dx.doi.org/10.1016/j.ijheatmasstransfer.2016.06.080.
[16] Y. Hao, X. Du, L. Yang, Y. Shen, Y. Yang, Numerical simulation of configuration and catalyst-layer effects on micro-channel steam reforming of methanol, Int. J. Hydrogen Energy 36 (2011) 15611–15621, http://dx.doi.org/10.1016/j.ijhydene.2011.09.038.
[17] R.-Y. Chein, L.-C. Chen, Y.-C. Chen, J.N. Chung, Heat transfer effects on the methanol-steam reforming with partially filled catalyst layers, Int. J. Hydrogen Energy 34 (2009) 5398–5408, http://dx.doi.org/10.1016/j.ijhydene.2009.04.049.
[18] R.-Y. Chein, Y.-C. Chen, J.N. Chung, Thermal resistance effect on methanol-steam reforming performance in micro-scale reformers, Int. J. Hydrogen Energy 37 (2012) 250–262, http://dx.doi.org/10.1016/j.ijhydene.2011.09.070.
[19] R.-Y. Chein, Y.-C. Chen, H.-J. Zhu, J.N. Chung, Numerical simulation of flow disturbance and heat transfer effects on the methanol-steam reforming in miniature annulus type reformers, Energy Fuels 26 (2012) 1202–1213, http://dx.doi.org/10.1021/ef201498t.
[20] R. Chein, Y.-C. Chen, J.N. Chung, Axial heat conduction and heat supply effects on methanol-steam reforming performance in micro-scale reformers, Int. J. Heat Mass Transfer 55 (2012) 3029–3042, http://dx.doi.org/10.1016/j.ijheatmasstransfer.2012.02.022.
[21] G. Arzamendi, P.M. Diéguez, M. Montes, J.A. Odriozola, E. Falabella Sousa-Aguiar, L.M. Gandía, Computational fluid dynamics study of heat transfer in a microchannel reactor for low-temperature Fischer-Tropsch synthesis, Chem. Eng. J. 160 (2010) 915–922, http://dx.doi.org/10.1016/j.cej.2009.12.028.
[22] N. Karimi, D. Agbo, A. Khan, P. Younger, On the effects of exothermicity and endothermicity upon the temperature fields in a partially-filled porous channel, Int. J. Therm. 96 (2015) 128–148.
[23] M. Torabi, N. Karimi, K. Zhang, Heat transfer and second law analyses of forced convection in a channel partially filled by porous media and featuring internal heat sources, Energy 93 (2015) 106–127, http://dx.doi.org/10.1016/j.energy.2015.09.010.
[24] M. Torabi, N. Karimi, K. Zhang, G.P. Peterson, Generation of entropy and forced convection of heat in a conduit partially filled with porous media – local thermal non-equilibrium and exothermicity effects, Appl. Therm. Eng. 106 (2016) 518–536, http://dx.doi.org/10.1016/j.applthermaleng.2016.06.036.
[25] C. Dickson, M. Torabi, N. Karimi, First and second law analyses of nanofluid forced convection in a partially-filled porous channel – the effects of local thermal non-equilibrium and internal heat sources, Appl. Therm. Eng. 103 (2016) 459–480, http://dx.doi.org/10.1016/j.applthermaleng.2016.04.095.
[26] M. Torabi, C. Dickson, N. Karimi, Theoretical investigation of entropy generation and heat transfer by forced convection of copper–water nanofluid in a porous channel — local thermal non-equilibrium and partial filling effects, Powder Technol. 301 (2016) 234–254, http://dx.doi.org/10.1016/j.powtec.2016.06.017.
[27] G. Ibáñez, A. López, J. Pantoja, J. Moreira, J. Reyes, Optimum slip flow based on the minimization of entropy generation in parallel plate microchannels, Energy 50 (2013) 143–149.
[28] M. Torabi, K. Zhang, Temperature distribution, local and total entropy generation analyses in MHD porous channels with thick walls, Energy 87 (2015) 540–554, http://dx.doi.org/10.1016/j.energy.2015.05.009.
[29] A. Elliott, M. Torabi, N. Karimi, S. Cunningham, On the effects of internal heat sources upon forced convection in porous channels with asymmetric thick walls, Int. Commun. Heat Mass Transfer 73 (2016) 100–110, http://dx.doi.org/10.1016/j.icheatmasstransfer.2016.02.016.
[30] B.R. Bakshi, T.G.P. Gutowski, D.P. Sekulić, Thermodynamics and the Destruction of Resources, Cambridge University Press, 2011.
[31] M. Torabi, K. Zhang, N. Karimi, G. Peterson, Entropy generation in thermal systems with solid structures – a concise review, Int. J. Heat. 97 (2016) 917–931.
[32] M. Mahdavi, M. Saffar-Avval, S. Tiari, Z. Mansoori, Entropy generation and heat transfer numerical analysis in pipes partially filled with porous medium, Int. J. Heat Mass Transfer 79 (2014) 496–506, http://dx.doi.org/10.1016/j.ijheatmasstransfer.2014.08.037.
[33] M. Siavashi, H.R. Talesh Bahrami, H. Saffari, Numerical investigation of flow characteristics, heat transfer and entropy generation of nanofluid flow inside an annular pipe partially or completely filled with porous media using two-phase mixture model, Energy 93 (2015) 2451–2466, http://dx.doi.org/10.1016/j.energy.2015.10.100.
[34] Y.S. Chee, T.W. Ting, Y.M. Hung, Entropy generation of viscous dissipative flow in thermal non-equilibrium porous media with thermal asymmetries, Energy 89 (2015) 382–401, http://dx.doi.org/10.1016/j.energy.2015.05.118.
[35] T. Ting, Y. Hung, N. Guo, Entropy generation of viscous dissipative nanofluid convection in asymmetrically heated porous microchannels with solid-phase heat generation, Energy Convers. Manage. 105 (2015) 731–745.
[36] D. Jiang, W. Yang, K.J. Chua, J. Ouyang, J.H. Teng, Analysis of entropy generation distribution in micro-combustors with baffles, Int. J. Hydrogen Energy 39 (2014) 8118–8125, http://dx.doi.org/10.1016/j.ijhydene.2014.03.092.
[37] S.Y. Jejurkar, D.P. Mishra, Numerical analysis of entropy generation in an annular microcombustor using multistep kinetics, Appl. Therm. Eng. 52 (2013) 394–401, http://dx.doi.org/10.1016/j.applthermaleng.2012.12.021.
[38] D. Jiang, W. Yang, J. Teng, Entropy generation analysis of fuel lean premixed CO/H_2/air flames, Int. J. Hydrogen Energy 40 (2015) 5210–5220, http://dx.doi.org/10.1016/j.ijhydene.2015.02.082.
[39] S.K. Som, A. Datta, Thermodynamic irreversibilities and exergy balance in combustion processes, Prog. Energy Combust. Sci. 34 (2008) 351–376, http://dx.doi.org/10.1016/j.pecs.2007.09.001.
[40] W.-H. Chen, T.-C. Cheng, C.-I. Hung, Modeling and simulation of microwave double absorption on methanol steam reforming for hydrogen production, Int. J. Hydrogen Energy 36 (2011) 333–344, http://dx.doi.org/10.1016/j.ijhydene.2010.09.009.

[41] S. Mahmud, R.A. Fraser, Flow, thermal, and entropy generation characteristics inside a porous channel with viscous dissipation, Int. J. Therm. Sci. 44 (2005) 21–32, http://dx.doi.org/10.1016/j.ijthermalsci.2004.05.001.
[42] G. Ibáñez, A. López, J. Pantoja, J. Moreira, Combined effects of uniform heat flux boundary conditions and hydrodynamic slip on entropy generation in a microchannel, Int. J. Heat Mass Transfer 73 (2014) 201–206, http://dx.doi.org/10.1016/j.ijheatmasstransfer.2014.02.007.
[43] G. Ibáñez, Entropy generation in MHD porous channel with hydrodynamic slip and convective boundary conditions, Int. J. Heat Mass Transfer 80 (2015) 274–280, http://dx.doi.org/10.1016/j.ijheatmasstransfer.2014.09.025.
[44] G. Ibáñez, A. López, J. Pantoja, J. Moreira, Entropy generation analysis of a nanofluid flow in MHD porous microchannel with hydrodynamic slip and thermal radiation, Int. J. Heat Mass Transfer 100 (2016) 89–97, http://dx.doi.org/10.1016/j.ijheatmasstransfer.2016.04.089.
[45] W.-H. Chen, T.-C. Cheng, C.-I. Hung, Numerical predictions on thermal characteristic and performance of methanol steam reforming with microwave-assisted heating, Int. J. Hydrogen Energy 36 (2011) 8279–8291, http://dx.doi.org/10.1016/j.ijhydene.2011.04.145.
[46] A. Amiri, K. Vafai, Analysis of dispersion effects and non-thermal equilibrium, non-Darcian, variable porosity incompressible flow through porous media, Int. J. Heat Mass Transfer 37 (1994) 939–954.
[47] B. Alazmi, K. Vafai, Analysis of variants within the porous media transport models, J. Heat Transfer 122 (2000) 303–326.
[48] A. Fan, J. Wan, Y. Liu, B. Pi, H. Yao, W. Liu, Effect of bluff body shape on the blow-off limit of hydrogen/air flame in a planar micro-combustor, Appl. Therm. Eng. 62 (2014) 13–19, http://dx.doi.org/10.1016/j.applthermaleng.2013.09.010.
[49] D.G. Norton, E.D. Wetzel, D.G. Vlachos, Fabrication of Single-Channel Catalytic Microburners: Effect of Confinement on the Oxidation of Hydrogen/Air Mixtures, 2004. doi:http://dx.doi.org/10.1021/IE049798B.
[50] K. Vafai, Handbook of Porous Media, CRC Press, 2015.
[51] M. Torabi, K. Zhang, G. Yang, J. Wang, P. Wu, Heat transfer and entropy generation analyses in a channel partially filled with porous media using local thermal non-equilibrium model, Energy 82 (2015) 922–938.
[52] M. Bovand, S. Rashidi, J.A. Esfahani, Heat transfer enhancement and pressure drop penalty in porous solar heaters: numerical simulations, Sol. Energy 123 (2016) 145–159, http://dx.doi.org/10.1016/j.solener.2015.10.054.
[53] X. Du, Y. Shen, L. Yang, Y. Shi, Y. Yang, Experiments on hydrogen production from methanol steam reforming in the microchannel reactor, Int. J. Hydrogen Energy 37 (2012) 12271–12280, http://dx.doi.org/10.1016/j.ijhydene.2012.06.027.